

# Modelling palaeoecological time series using generalized additive models

Gavin L. Simpson

[gavin.simpson@uregina.ca](mailto:gavin.simpson@uregina.ca)<sup>1</sup>

<sup>1</sup>Institute of Environmental Change and Society, University of Regina,  
Regina, Saskatchewan, Canada, S4S 0A2

August 16, 2018

*Keywords*— time series; generalized additive model; simultaneous interval; spline; environmental change

## Abstract

In the absence of annual laminations, time series generated from lake sediments or other similar stratigraphic sequences are irregularly spaced in time, which complicates formal analysis using classical statistical time series models. In lieu, statistical analyses of trends in palaeoenvironmental time series, if done at all, have typically used simpler linear regressions or (non-) parametric correlations with little regard for the violation of assumptions that almost surely occurs due to temporal dependencies in the data or that correlations do not provide estimates of the magnitude of change, just whether or not there is a linear or monotonic trend. Alternative approaches have used LOESS-estimated trends to justify data interpretations or test hypotheses as to the causal factors without considering the inherent subjectivity of the choice of parameters used to achieve the LOESS fit (e.g. span width, degree of polynomial). Generalized additive models (GAMs) are statistical models that can be used to estimate trends as smooth functions of time. Unlike LOESS, GAMs use automatic smoothness selection methods to objectively determine the complexity of the fitted trend, and as formal statistical models, GAMs, allow for potentially complex, non-linear trends, a proper accounting of model uncertainty, and the identification of periods of significant temporal change. Here, I present a consistent and modern approach to the estimation of trends in palaeoenvironmental time series using GAMs, illustrating features of the methodology with two example time series of contrasting complexity; a 150-year bulk organic matter  $\delta^{15}\text{N}$  time series from Small Water, UK, and a 3000-year alkenone record from Braya-Sø, Greenland. I discuss the underlying mechanics of GAMs that allow them to learn the shape of the trend from the data themselves and how simultaneous confidence intervals and the first derivatives of the trend are used to properly account for

32 model uncertainty and identify periods of change. It is hoped that by using GAMs greater at-  
33 tention is paid to the statistical estimation of trends in palaeoenvironmental time series leading  
34 to more a robust and reproducible palaeoscience.

## 35 1 Introduction

36 Palaeoecology and palaeolimnology have moved away from being descriptive disciplines,  
37 rapidly adopting new statistical developments in the 1990s and beyond (Smol et al., 2012).  
38 Less development has been observed in the area of trend estimation in palaeoenvironmental  
39 time series. The vast majority of data produced by palaeoecologists and palaeolimnologists  
40 is in the form of time-ordered observations on one or more proxies or biological taxa (Birks,  
41 2012b; Smol, 2008; Smol et al., 2012). Typically these data are arranged irregularly in time;  
42 in the absence of annual laminae or varves, the sediment core is sectioned at regular depth  
43 intervals (Glew et al., 2001), which, owing to variation in accumulation rates over time  
44 and compaction by overlying sediments, results in an uneven sampling in time. An under-  
45 appreciated feature of such sampling is that younger sediments often have larger variance  
46 than older sediments; each section of core represents fewer lake years in newer samples,  
47 relative to older samples. This variable averaging acts as a time-varying low-pass (high-cut)  
48 filter of the annual depositional signal.

49 Irregular intervals between samples means that the time-series analysis methods of autore-  
50 gressive or moving average processes, in the form of autoregressive integrated moving aver-  
51 age (ARIMA) models, are practically impossible to apply because software typically requires  
52 even spacing of observations in time. Dutilleul et al. (2012) and Birks (2012a), eschewing the  
53 term *time series*, prefer to call such data *temporal series* on account of the irregular spacing of  
54 samples, a distinction that I find unnecessary, however.

55 Where statistical approaches have been applied to trend estimation in palaeoenvironmental  
56 time series, a commonly-used method is LOESS (Birks, 1998, 2012a; Cleveland, 1979; Juggins  
57 and Telford, 2012). LOESS, locally weighted scatterplot smoother, as it's name suggests, was  
58 developed to smooth x-y scatterplot data (Cleveland, 1979). The method fits a smooth line  
59 through data by fitting weighted least squares (WLS) models to observations within a user-  
60 specified window of the focal point, whose width is typically expressed as a proportion  $\alpha$  of  
61 the  $n$  data points. Weights are determined by how close (in the x-axis only) an observation in  
62 the window is to the focal point giving greatest weight given to points closest to the focal point.  
63 The interim LOESS-smoothed value for the focal point is the predicted value from the weighted  
64 regression at the focal point. The interim values are updated using weights based on how far  
65 in the y-axis direction the interim smoothed value lies from the observed value plus the x-axis  
66 distance weights; this has the effect of down-weighting outlier observations. The final LOESS is  
67 obtained by joining the smoothed values. The user has to choose how large a window to use,  
68 whether to fit degree 1 (linear) or degree 2 (quadratic) polynomials in the WLS model, and how  
69 to weight points in the x-axis. When used in an exploratory mode, the user has considerable  
70 freedom to choose the detail of the LOESS fit; the window width, for example, can be infinitely  
71 tweaked to give as close a fit to the data, as assessed by eye, as is desired. Using cross-validation  
72 (CV) to choose  $\alpha$  or the degree of polynomial in the WLS model is complicated for a number of

73 reasons, not least because the CV scheme used must involve the time ordering of the data (e.g.  
74 Bergmeir et al., 2018). This subjectivity is problematic however once we wish to move beyond  
75 exploratory analysis and statistically identify trends to test hypotheses involving those trend  
76 estimates.

77 Running means or other types of filter (Juggins and Telford, 2012) have also been used exten-  
78 sively to smooth palaeoenvironmental time series, but, as with LOESS, their behaviour depends  
79 on a number of factors, including the filter width. Furthermore, the width of the filter causes  
80 boundary issues; with a centred filter, of width five, the filtered time series would be two data  
81 points shorter at both ends of the series because the filter values are not defined for the first  
82 and last two observations of the original series as these extra time points were not observed.  
83 Considerable research effort has been expended to identify ways to pad the original time series  
84 at one or both ends to maintain the original length in the filtered series, without introducing  
85 bias due to the padding (e.g. Mann, 2004, 2008; Mills, 2006, 2007, 2010).

86 These are not the only methods that have been used to estimated trends in stratigraphic series.  
87 Another common approach involves fitting a simple linear trend using ordinary least squares  
88 regression and use the resulting  $t$  statistic as evidence against the null hypothesis of no trend  
89 despite the statistical assumptions being almost surely violated due to dependence among  
90 observations. The Pearson correlation coefficient,  $r$ , is also often used to detect trends in palaeo  
91 time series (Birks, 2012a), despite the fact that  $r$  provides no information as to the magnitude of  
92 the estimated trend, and the same temporal autocorrelation problem that dogs ordinary least  
93 squares similarly plagues significance testing for  $r$  (Tian et al., 2011). Additionally, both the  
94 simple least squares trend line and  $r$  are tests for *linear* trends only, and yet we typically face  
95 data sets with potentially far more complex trends than can be identified by these methods.  
96 Instead, non-parametric rank correlation coefficients have been used (Birks, 2012a; Gautheir,  
97 2001), and whilst these do allow for the detection of non-linear trends, trends are restricted to  
98 be monotonic, no magnitude of the trend is provided, and the theory underlying significance  
99 testing of Spearman's  $\rho$  and Kendall's  $\tau$  assumes independent observations.

100 Here, I describe generalized additive models (GAMs; Hastie and Tibshirani, 1986, 1990; Rup-  
101 pert et al., 2003; Wood, 2017; Yee and Mitchell, 1991) for trend estimation. GAMs, like simple  
102 linear regression, are a regression-based method for estimating trends, yet they are also, su-  
103 perfluentially at least, similar to LOESS. GAMs and LOESS estimate smooth, non-linear trends in  
104 time series and both can handle the irregular spacing of samples in time, yet GAMs do not  
105 suffer from the subjectivity that plagues LOESS as a method of formal statistical inference.

106 In the subsequent sections, I present an introduction to GAMs and discuss the issue of uncer-  
107 tainty in model-estimated trends, the topic of posterior simulation from a regression model  
108 and how to identify periods of significant environmental change using the first derivative of  
109 the estimated trend. The main steps in the analysis of palaeoenvironmental time series using  
110 GAMs are illustrated in Figure 1. Two non-standard types of spline — adaptive smoothers and  
111 Gaussian process splines — that are especially applicable to GAMs in the palaeoenvironmental  
112 setting are subsequently described, followed by an assessment of the the impact of age-model  
113 uncertainty on trend estimation via GAMs. Finally, I briefly discuss the application of GAM  
114 trend analysis to multivariate species abundance and compositional data.

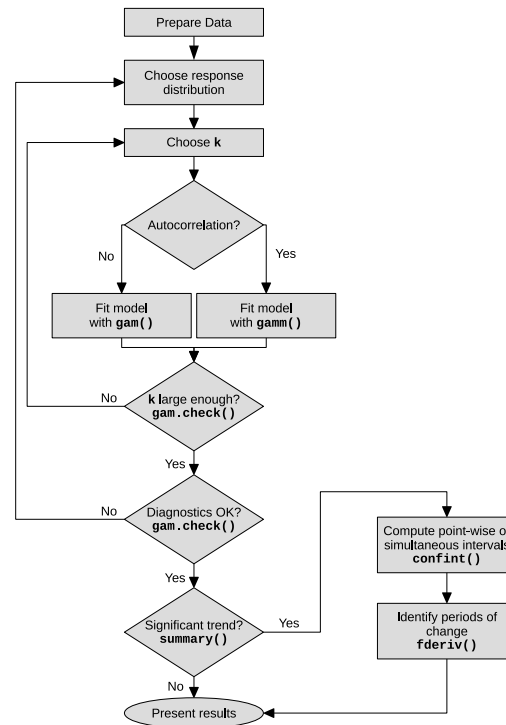


Figure 1: Flowchart showing the main steps in the analysis of time series using generalized additive models. The main R functions associated with each step or decision are shown in bold.

## 1.1 Example time series

To illustrate trend estimation in palaeoenvironmental data using GAMs, I use two proxy time series; a 150-year bulk organic matter  $\delta^{15}\text{N}$  record from Small Water, and a 3000-year alkenone record from Braya-Sø. Between them, the two examples, combine many of the features of interest to palaeoecologists that motivate the use of GAMs; non-linear trends and the question of when changes in the measured proxy occurred. The example analyses were all performed using the *mgcv* package (version 1.8.24; Wood, 2017) and R (version 3.4.4; R Core Team, 2018), and the supplementary material contains a fully annotated document showing the R code used to replicate all the analyses described in the remainder of the paper.

### 1.1.1 $\delta^{15}\text{N}$ time series from Small Water

Figure 2a shows 48 nitrogen stable isotope measurements on the bulk organic matter of a sediment core collected from Small Water, a small corrie lake located in the English Lake District, UK. The data were collected to investigate disturbance of nitrogen (N) cycling in remote, oligotrophic lakes by N deposited from the atmosphere (Simpson, unpublished data). The data are shown on a  $^{210}\text{Pb}$  time scale. Questions that might be asked about this series are; what is the trend in  $\delta^{15}\text{N}$ ?, when do we first see evidence for a change in  $\delta^{15}\text{N}$ ?, and is the reversal in  $\delta^{15}\text{N}$  values in the uppermost section of the core a real change?

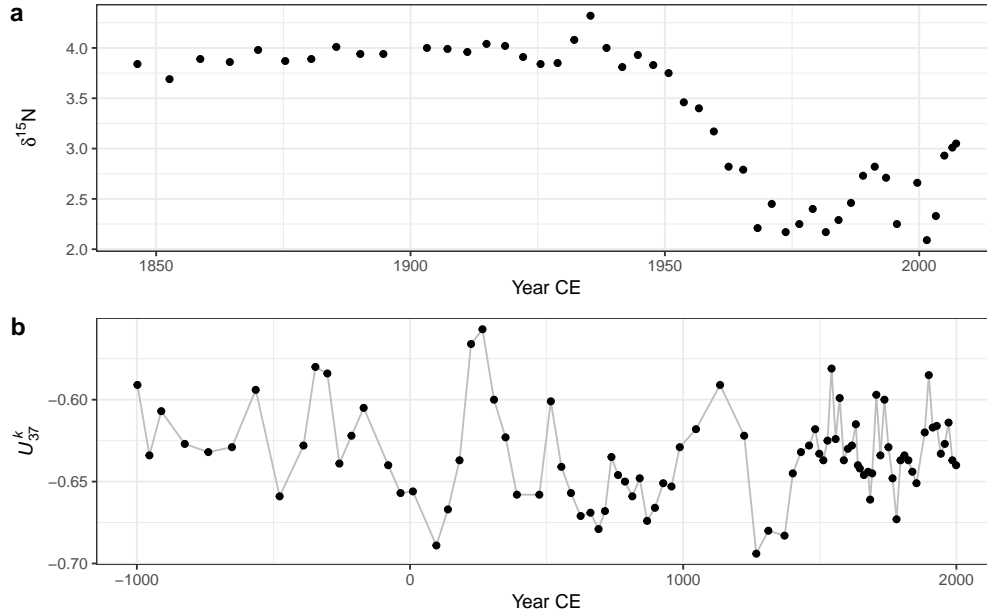


Figure 2: Example time series; a) Small Water bulk organic matter  $\delta^{15}\text{N}$  time series on a  $^{210}\text{Pb}$  time scale, and b) Braya-Sø  $U_{37}^K$  time series on a calibrated  $^{14}\text{C}$  time scale. The observations  $U_{37}^K$  time series have been joined by lines purely as a visual aid to highlight potential trends.

### 132 1.1.2 Braya-Sø alkenone time series

133 The second example time series is a 3,000 year record of alkenone unsaturation,  $U_{37}^K$ , from  
 134 Braya-Sø, a meromictic lake in West Greenland (D'Andrea et al., 2011). Alkenones are long-  
 135 chained unsaturated organic compounds that are produced by a small number of planktonic  
 136 organisms known as haptophytes. The  $U_{37}^K$  unsaturation index (Brassell, 1993) is

$$U_{37}^K = \frac{[C_{37:2}] - [C_{37:4}]}{[C_{37:2}] + [C_{37:3}] + [C_{37:4}]}$$

137 where  $[C_{37:x}]$  is the concentration of the alkenone with 37 carbon atoms and  $x$  double carbon  
 138 bonds. The relative abundance of these alkenones is known to vary with changes in water  
 139 temperature (Brassell, 1993; Chu et al., 2005; Toney et al., 2010; Zink et al., 2001), and as a  
 140 result  $U_{37}^K$  is used as a proxy for lake- and sea-surface temperatures. For further details on the  
 141 Braya-Sø  $U_{37}^K$  record and age model see D'Andrea et al. (2011). Here I use the 3,000 year  $U_{37}^K$   
 142 record from the PAGES 2K database (PAGES 2K Consortium, 2013). The data are presented in  
 143 Figure 2b.

## 144 2 Regression models for palaeoenvironmental time series

145 A linear model for a trend in a series of  $T$  observations  $y_t$  at observation times  $x_t$  with  $t =$   
 146  $1, 2, \dots, T$  is

$$y_t = \beta_0 + \beta_1 x_t + \varepsilon_t, \quad (1)$$

147 where  $\beta_0$  is a constant term, the model *intercept*, representing the expected value of  $y_t$  where  
148  $x_t$  is 0.  $\beta_1$  is the *slope* of the best fit line through the data; it measures the rate of change in  $y$   
149 for a unit increase in  $x$ . The unknowns, the  $\beta_j$ , are commonly estimated using least squares  
150 by minimising the sum of squared errors,  $\sum_t \varepsilon_t^2$ . If we want to ask if the estimated trend  $\beta_1$  is  
151 statistically significant we must make further assumptions about the data (conditional upon  
152 the fitted model) or the model errors (residuals);  $\varepsilon_t \stackrel{iid}{\sim} \mathcal{N}(0, \sigma^2)$ . This notation indicates that  
153 the residuals  $\varepsilon_t$  are *independent* and *identically distributed* Gaussian random variables with mean  
154 equal to 0 and constant variance  $\sigma^2$ . In the time series setting, the assumption of independence  
155 of model residuals is often violated.

156 The linear model described above is quite restrictive in terms of the types of trend it can fit;  
157 essentially linear increasing or decreasing trends, or, trivially, a null trend of no change. This  
158 model can be extended to allow for non-linear trends by making  $y_t$  depend on polynomials of  
159  $x_t$ , for example

$$\begin{aligned} y_t &= \beta_0 + \beta_1 x_t + \beta_2 x_t^2 + \dots + \beta_P x_t^P + \varepsilon_t \\ &= \beta_0 + \sum_{p=1}^P \beta_p x_t^p + \varepsilon_t, \end{aligned} \quad (2)$$

160 where polynomials of  $x_t$  up to order  $P$  are used. This model allows for more complex trends  
161 but it remains a fully parametric model and suffers from several problems, especially the be-  
162 haviour of the fitted trend at the start and end of the observed series.

163 Linear models using a range of polynomials fitted to the Small Water data set are shown in  
164 Figure 3. The low-order models ( $P \in \{1, 3\}$ ) result in very poor fit to the data. The model with  
165  $P = 5$  does a reasonable job of capturing the gross pattern in the time series, but fails to adapt  
166 quickly enough to the decrease in  $\delta^{15}\text{N}$  that begins  $\sim 1940$  CE, and the estimated trend is quite  
167 biased as a result. The  $P = 10$ th-order polynomial model is well able to capture this period  
168 of rapid change, but it does so at the expense of increased complexity in the estimated trend  
169 prior to  $\sim 1940$ . Additionally, this model ( $P = 10$ ) has undesirable behaviour at the ends of the  
170 series, significantly overfitting the data, a commonly observed problem in polynomial models  
171 such as these (Epperson, 1987; Runge, 1901). Finally, the choice of what order of polynomial to  
172 fit is an additional choice left for the analyst to specify; choosing the optimal  $P$  is not a trivial  
173 task when the data are a time series and residual autocorrelation is likely present.

174 Can we do better than these polynomial fits? In the remainder, I hope to demonstrate that  
175 the answer to that question is emphatically “yes”! Below I describe a coherent and consistent  
176 approach to modelling palaeoenvironmental time series using generalized additive models  
177 that builds upon the linear regression framework.

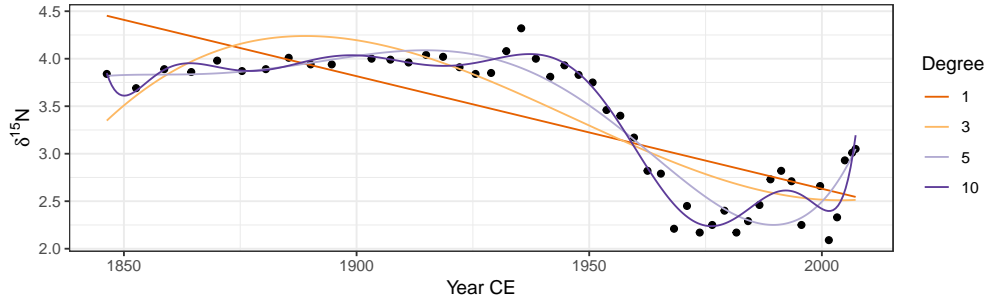


Figure 3: Linear models with various orders of polynomial of the covariate Year fitted using ordinary least squares to the  $\delta^{15}\text{N}$  time series from Small Water. The degree of polynomial is indicated, with the degree 1 line equal to a simple linear regression model.

### 178 3 Generalized additive models

179 The GAM version of the linear model (1) is

$$y_t = \beta_0 + f(x_t) + \varepsilon_t, \quad (3)$$

180 where the linear effect of time (the  $\beta_1 x_t$  part) has been replaced by a smooth function of time,  
 181  $f(x_t)$ . The immediate advantage of the GAM is that we are no longer restricted to the shapes  
 182 of trends that can be fitted via global polynomial functions such as (2). Instead, the shape of  
 183 the fitted trend will be estimated from the data itself.

184 The linear model is a special case of a broader class, known as the generalized linear model  
 185 (GLM; McCullagh and Nelder, 1989). The GLM provides a common framework for modelling  
 186 a wide range of types of data, such as count, proportions, or binary (presence/absence) data,  
 187 that are not conditionally distributed Gaussian. GLMs are, like the linear model, parametric  
 188 in nature; the types of trends that we can fit using a GLM are the linear or polynomial mod-  
 189 els. GAMs extend the GLM by relaxing this parametric assumption; in a GAM some, or all,  
 190 of the parametric terms, the  $\beta_p$ , are replaced by smooth functions  $f_j$  of the covariates  $x_j$ . For  
 191 completeness then, we can write (3) as a GLM/GAM

$$y_t \sim \text{EF}(\mu_t, \Theta) \quad (4a)$$

$$g(\mu_t) = \beta_0 + f(x_t) \quad (4b)$$

$$\mu_t = g^{-1}(\beta_0 + f(x_t)), \quad (4c)$$

192 where  $\mu_t$  is the expected value (e.g. the mean count or the probability of occurrence) of the  
 193 random variable  $Y_t$  ( $\mu_t \equiv \mathbb{E}(Y_t)$ ) of which we have observations  $y_t$ .  $g$  is the link function, an  
 194 invertible, monotonic function, such as the natural logarithm, and  $g^{-1}$  is its inverse. The link  
 195 function maps values from the response scale on to the scale of the linear predictor, whilst the  
 196 inverse of the link function provides the reverse mapping. For example, count data are strictly  
 197 non-negative integer values and are commonly modelled as a Poisson GLM/GAM using the

198 natural log link function. On the log scale, the response can take any real value between  $-\infty$   
199 and  $+\infty$ , and it is on this scale that model fitting actually occurs (i.e. using equation (4b)).  
200 However we need to map these unbounded values back on to the non-negative response scale.  
201 The inverse of the log link function, the exponential function, achieves this and maps values  
202 to the interval  $0-\infty$  (equation (4c)).

203 In (4a), we further assume that the observations are drawn from a member of the exponential  
204 family of distributions — such as the Poisson for count data, the binomial for presence/absence  
205 or counts from a total — with expected value  $\mu_t$  and possibly some additional parameters  $\Theta$   
206 ( $y_t \sim \text{EF}(\mu_t, \Theta)$ ). Additionally, many software implementations of the above model also allow  
207 for distributions that are not within the exponential family but which can be fitted using an  
208 algorithm superficially similar to the one used to fit GAMs to members of the exponential  
209 family (e.g. Wood et al., 2016). Common examples of such extended families include the  
210 negative binomial distribution (for overdispersed counts) and the beta distribution (for true  
211 proportions or other interval-bounded data).

### 212 3.1 Basis functions

213 It is clear from plots of the data (Figure 2) that we require the fitted trends for the Small Water  
214  $\delta^{15}\text{N}$  and Braya-Sø  $U_{37}^K$  time series to be non-linear functions, but it is less clear how to specify  
215 the actual shape require. Ideally, we'd like to learn the shape of the trend from the data them-  
216 selves. We will refer to these non-linear functions as *smooth functions*, or just *smooths* for short,  
217 and we will denote a smooth using  $f(x_t)$ . Further, we would like to represent the smooths in  
218 a way that (4) is represented parametrically so that it can be estimate within the well-studied  
219 GLM framework. This is achieved by representing the smooth using a *basis*. A basis is a set  
220 of functions that collectively span a space of smooths that, we hope, contains the true  $f(x_t)$  or  
221 a close approximation to it. The functions in the basis are known as *basis functions*, and arise  
222 from a *basis expansion* of a covariate. Writing  $b_j(x_t)$  as the  $j$ th basis function of  $x_t$ , the smooth  
223  $f(x_t)$  can be represented as a weighted sum of basis functions

$$f(x_t) = \sum_{j=1}^k b_j(x_t)\beta_j,$$

224 where  $\beta_j$  is the weight applied to the  $j$ th basis function.

225 The polynomial model is an example of a statistical model that uses a basis expansion. For the  
226 cubic polynomial ( $P = 3$ ) fit shown in Figure 3 there are in fact 4 basis functions:  $b_1(x_t) = x_t^0 = 1$ ,  
227  $b_2(x_t) = x_t$ ,  $b_3(x_t) = x_t^2$ , and  $b_4(x_t) = x_t^3$ . Note that  $b_1(x_t)$  is constant and is linked to the  
228 model intercept,  $\beta_0$ , in the linear model (2), and further, that the basis function weights are the  
229 estimated coefficients in the model, the  $\beta_j$ .

230 As we have already seen, polynomial basis expansions do not necessarily lead to well-fitting  
231 models unless the true function  $f$  is itself a polynomial. One of the primary criticisms is that  
232 polynomial basis functions are global (Magee, 1998); the value of  $f$  at time point  $x_t$  affects the  
233 value of  $f$  at time point  $x_{t+s}$  even if the two time points are at opposite ends of the series. There  
234 are many other bases we could use; here I discuss one such set of bases, that of splines.



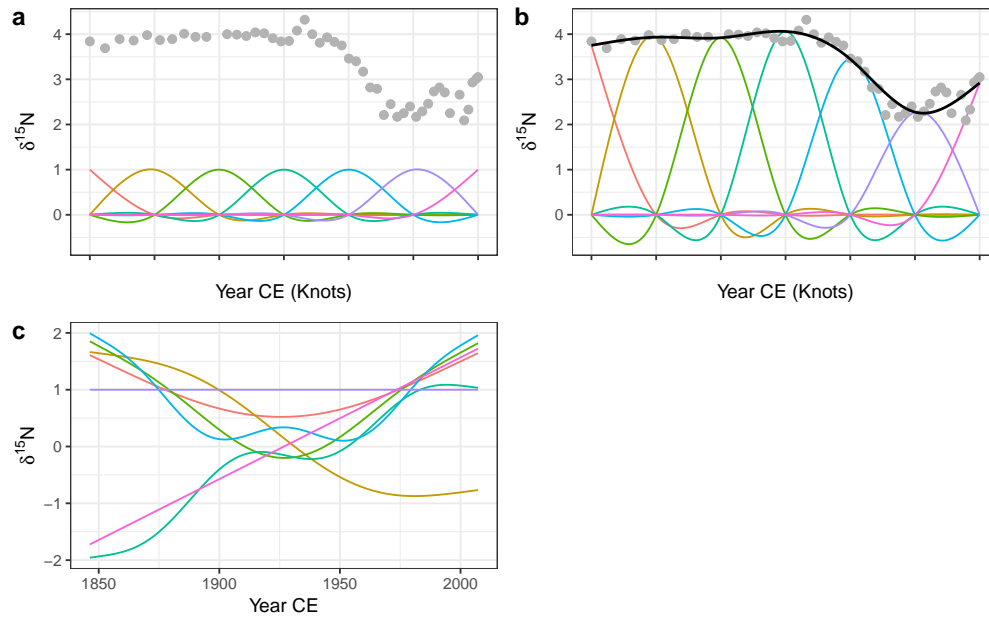


Figure 4: Basis functions for the time covariate and the Small Water  $\delta^{15}\text{N}$  time series. A rank (size) 7 cubic regression spline (CRS) basis expansion is shown in a), with knots, indicated by tick marks on the x-axis, spread evenly through the range of the data. b) shows the same CRS basis functions weighted by the estimated coefficients  $\beta_j$ , plus the resulting GAM trend line (black line drawn through the data). The grey points in both panels are the observed  $\delta^{15}\text{N}$  values. c) A rank 7 thin plate regression spline basis for the same data.

235 There are a bewildering array of different types of spline. In the models discussed below we  
236 will largely restrict ourselves to cubic regression splines (CRS) and thin plate regression splines  
237 (TPRS). In addition, I also discuss two special types of spline basis, an adaptive spline basis  
238 and a Gaussian process spline basis.

239 A cubic spline is a smooth curve comprised of sections of cubic polynomials, where the sections  
240 are joined together at some specified locations — known as *knots* — in such a way that at  
241 the joins, the two sections of cubic polynomial that meet have the same value as well as the  
242 same first and second derivative. These properties mean that the sections join smoothly and  
243 differentiably at the knots (Wood, 2017, 5.3.1).

244 The CRS can be parameterized in a number of different ways. One requires a knot at each  
245 unique data value in  $x_t$ , which is computationally inefficient. Another way of specifying a  
246 CRS basis is to parameterize in terms of the value of the spline at the knots. Typically in  
247 this parametrization there are many fewer knots than unique data, with the knots distributed  
248 evenly over the range of  $x_t$  or at the quantiles of  $x_t$ . Placing knots at the quantiles of  $x_t$  has the  
249 effect of placing a greater number of knots where the data is most dense.

250 A CRS basis expansion comprised of 7 basis functions for the time covariate in the Small Water  
251 series, is shown in Figure 4a. The tick marks on the x-axis show the locations of the knots,  
252 which are located at the ends of the series and evenly in between. Notice that in this particular  
253 parametrization, the  $j$ th basis function takes a value of 1 at the  $j$ th knot and at all other knots

254 a value of 0.

255 To estimate a model using this basis expansion each basis function forms a column in the model  
256 matrix  $\mathbf{X}$  and the weights  $\beta_j$  can be found using least squares regression (assuming a Gaussian  
257 response). Note that in order to estimate a coefficient for each basis function the model has  
258 to be fitted without an intercept term. In practice we would include an intercept term in the  
259 model and therefore the basis functions are modified via an identifiability constraint (Wood,  
260 2017). This has the effect of making the basis orthogonal to the intercept but results in more  
261 complicated basis functions than those shown in in Figure 4a.

262 Having estimated the weight for each basis function, the  $j$ th basis function  $b_j$  is scaled  
263 (weighted) by its coefficient  $\beta_j$ . The scaled CRS basis functions for the Small Water time series  
264 are shown in Figure 4b. The solid line passing through the data points is formed by summing  
265 up the values of the seven scaled basis functions ( $b_j(x_t)\beta_j$ ) at any value of  $x_t$  (time).

266 Cubic regression splines, as well as many other types of spline, require the analyst to choose  
267 the number and location of the knots that parametrise the basis. Thin plate regression splines  
268 (TPRS) remove this element of subjectivity when fitting GAMs. Thin plate splines were in-  
269 troduced by Duchon (1977) and, as well as solving the knot selection problem, have several  
270 additional attractive properties in terms of optimality and their ability to estimate a smooth  
271 function of two or more variables, leading to smooth interactions between covariates. How-  
272 ever, thin plate splines have one key disadvantage over CRS; thin plate splines have as many  
273 unknown parameters as there are unique combinations of covariate values in a data set (Wood,  
274 2017, 5.5.1). It is unlikely that any real data problem would involve functions of such complex-  
275 ity that they require as many basis functions as data. It is much more likely that the true func-  
276 tions that we attempt to estimate are far simpler than the set of functions representable by 1  
277 basis function per unique data value. From a practical point of view, it is also highly inefficient  
278 to carry around all these basis functions whilst model fitting, and the available computational  
279 resources would become quickly exhausted for large time series with many observations.

280 To address this issue low rank thin plate regression splines (TPRS) have been suggested which  
281 truncate the space of the thin plate spline basis to some lower number of basis functions whilst  
282 preserving much of the advantage of the original basis as an optimally-fitting spline (Wood,  
283 2003). A rank 7 TPRS basis (i.e. one containing 7 basis functions) is shown in Figure 4c for the  
284 Small Water time series. The truncation is achieved by performing an eigen-decomposition  
285 of the basis functions and retaining the eigenvectors associated with the  $k$  largest eigenvalues.  
286 This is similar to the way principal components analysis decomposes a data set into axes of  
287 variation (eigenvectors) in decreasing order of variance explained. The truncated basis can  
288 preserve much of the space of functions spanned by the original basis but at the cost of using  
289 far fewer basis functions (Wood, 2003, 2017, 5.5.1). Note the horizontal TPRS basis function (at  
290  $\delta^{15}\text{N} = 1$ ) in Figure 4c; this basis function is confounded with the intercept term and, after the  
291 application of identifiability constraints, ends up being removed from the set of basis functions  
292 used to fit the model.

293 The truncation suggested by Wood (2003) is not without cost; the eigen-decomposition and  
294 related steps can be relatively costly for large data sets. For data sets of similar size to the two  
295 examples used here, the additional computational effort required to set up the TPRS basis over  
296 the CRS basis will not be noticeable. For highly resolved series containing more than  $\sim 1000$

297 observations the truncation may be costly computationally. In such instances, little is lost by  
298 moving to the CRS basis with the same number of knots as the rank of the desired TPRS, with  
299 the benefit of considerably reduced set up time for the basis.

300 To fit a GAM using either of the two regression spline bases described above, the analyst is  
301 generally only required to specify the size (rank) of the basis expansion required to rep-  
302 resent or closely approximate the true function  $f$ . With practice and some knowledge of the  
303 system from which the observations arise, it can be relatively easy to put an upper limit on the  
304 expected complexity of the true trend in the data. Additionally, the number of available data  
305 points places a constraint on the upper limit of the size of basis expansion that can be used.

306 In practice, the size of the basis is an upper limit on the expected complexity of the trend,  
307 and a simple test can be used to check if the basis used was sufficiently large (Pya and Wood,  
308 2016). This test is available via the `gam.check()` function in `mgcv` for example, which essen-  
309 tially looks at whether there is any additional nonlinearity or structure in the residuals that  
310 can be explained by a further smooth of  $x_t$ . Should a smooth term in the fitted model fail this  
311 test the model can be refitted using a larger basis expansion, say by doubling the value of  $k$  (the  
312 rank) used to fit the original. Note also that a smooth might fail this test whilst using fewer  
313 effective degrees of freedom than the maximum possible for the dimension of basis used. This  
314 may happen when the true function lies at the upper limit of the set of functions encompassed  
315 by the size of basis used. Additionally, a basis of size  $2k$  encompasses a richer space of func-  
316 tions of a given complexity than a basis of size  $k$  (Wood, 2017); increasing the basis dimension  
317 used to fit the model may unlock this additional function space resulting in a better fitting  
318 model whilst using a similar number of effective degrees of freedom.

## 319 3.2 Smoothness selection

320 Having identified low rank regression splines as a useful way to represent  $f$ , we next need  
321 a way to decide how wiggly the fitted trend should be. A backwards elimination approach  
322 to sequentially remove knots or basis functions might seem appropriate, however such an  
323 approach would likely fail as the resulting sequence of models would not be strictly nested,  
324 precluding many forms of statistical comparison (Wood, 2017). Alternatively, we could keep  
325 the basis dimension at a fixed size but guard against fitting very complex models through the  
326 use of a wiggleness penalty.

327 The default wiggleness penalty used in GAMs is on the second derivative of the spline, which  
328 measures the rate of change of the slope, or the curvature, of the spline at any infinitesimal  
329 point in the interval spanned by  $x_t$ . The actual penalty used is the integrated squared second  
330 derivative of the spline

$$\int_{\mathbb{R}} [f'']^2 dx = \beta^T \mathbf{S} \beta. \quad (5)$$

331 The right hand side of (5) is the penalty in quadratic form. The convenience of the quadratic  
332 form is that it is a function of the estimated coefficients of  $f(x_t)$  where  $\mathbf{S}$  is known as the penalty  
333 matrix. Notice that now both the weights for the basis functions and the wiggleness penalty  
334 are expressed as functions of the model coefficients.

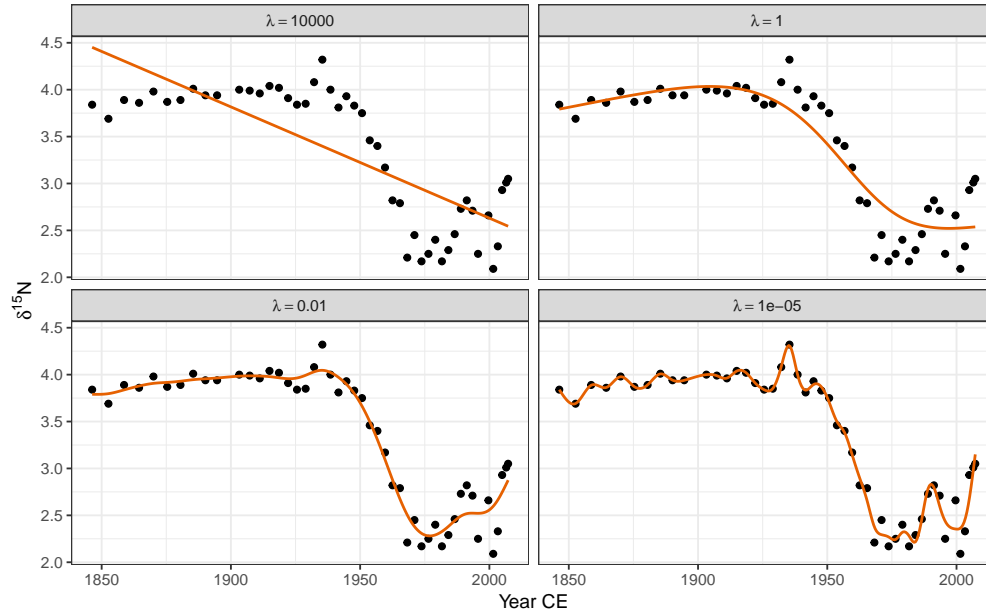


Figure 5: The effect of the smoothness parameter  $\lambda$  on the resulting wiggleness of the estimated spline. Large values of  $\lambda$  penalize wiggleness strongly, resulting in smooth trends (upper row), while smaller values allow increasingly wiggly trends. The aim of automatic smoothness selection is to find an optimal value of  $\lambda$  that balances the fit of the model with model complexity to avoid overfitting.

335 Now that we have a convenient way to measure wiggleness, it needs to be incorporated into  
 336 the objective function that will be minimised to fit the GAM. The likelihood of the model given  
 337 the parameter estimates  $\mathcal{L}(\beta)$  is combined with the penalty to create the penalized likelihood  
 338  $\mathcal{L}_p(\beta)$ :

$$\mathcal{L}_p(\beta) = \mathcal{L}(\beta) - \frac{1}{2}\lambda\beta^T\mathbf{S}\beta.$$

339 The fraction of a half is there simply to make the penalised likelihood equal the penalised  
 340 sum of squares in the case of a Gaussian model.  $\lambda$  is known as the smoothness parameter  
 341 and controls the extent to which the penalty contributes to the likelihood of the model. In  
 342 the extreme case of  $\lambda = 0$  the penalty has no effect and the penalized likelihood equals the  
 343 likelihood of the model given the parameters. At the other extreme, as  $\lambda \rightarrow \infty$  the penalty  
 344 comes to dominate  $\mathcal{L}_p(\beta)$  and the wiggleness of  $f(x_t)$  tends to 0 resulting in an infinitely smooth  
 345 function. In the case of a second derivative penalty, this is a straight line, and we recover the  
 346 simple linear trend from (1) when assuming a Gaussian response.

347 Figure 5 illustrates how the smoothness parameter  $\lambda$  controls the degree of wiggleness in the  
 348 fitted spline. Four models are shown, each fitted with a fixed value of  $\lambda$ ; 10000, 1, 0.01, and  
 349 0.00001. At  $\lambda = 10000$  the model effectively fits a linear model through the data. As the value  
 350 of  $\lambda$  decreases, the fitted spline becomes increasingly wiggly. As  $\lambda$  becomes very small, the  
 351 resulting spline passes through most of the  $\delta^{15}\text{N}$  observations resulting in a model that is  
 352 clearly over fitted to the data.

353 To fully automate smoothness selection for  $f(x_t)$  we need to estimate  $\lambda$ . There are two main  
354 ways that  $\lambda$  can be automatically chosen during model fitting. The first way is to choose  $\lambda$   
355 such that it minimises the prediction error of the model. This can be achieved by choosing  $\lambda$   
356 to minimise Akaike's information criterion (AIC) or via cross-validation (CV) or generalized  
357 cross-validation (GCV; Craven and Wahba, 1978). GCV avoids the computational overhead  
358 inherent to CV of having to repeatedly refit the model with one or more observations left out  
359 as a test set. Minimising the GCV score will, with a sufficiently large data set, find a model  
360 with the minimal prediction error (Wood, 2017). The second approach is to treat the smooth  
361 as a random effect, in which  $\lambda$  is now a variance parameter to be estimated using maximum  
362 likelihood (ML) or restricted maximum likelihood (REML; Wood, 2011; Wood et al., 2016).

363 Several recent results have shown that GCV, under certain circumstances, has a tendency to  
364 under smooth, resulting in fitted splines that are overly wiggly (Reiss and Ogden, 2009). Much  
365 better behaviour has been observed for REML and ML smoothness selection, in that order  
366 (Wood, 2011). REML is therefore the recommended means of fitting GAMs, though, where  
367 models have different fixed effects (covariates) they cannot be compared using REML, and  
368 ML selection should be used instead. In the sorts of data examples considered here there is  
369 only a single covariate  $x_t$  as our models contain a single estimated trend so REML smoothness  
370 selection is used throughout unless otherwise stated.

## 371 4 Fitting GAMs

### 372 4.1 Small Water

373 The trend in  $\delta^{15}\text{N}$  values is clearly non-linear but it would be difficult to suggest a suitable  
374 polynomial model that would allow for periods of relatively no change in  $\delta^{15}\text{N}$  as well as rapid  
375 change. Instead, a GAM is ideally suited to modelling such trends; the data suggest a smoothly  
376 varying change in  $\delta^{15}\text{N}$  between 1925 and 1975. It is reasonable to expect some autocorrelation  
377 in the model errors about the fitted trend. Therefore I fitted the following GAM to the  $\delta^{15}\text{N}$   
378 time series.

$$y_t = \beta_0 + f(x_t) + \varepsilon, \quad \varepsilon_t \sim (0, \Lambda\sigma^2) \quad (6)$$

379 Now the i.i.d. assumption has been relaxed and a correlation matrix,  $\Lambda$ , has been introduced  
380 that is used to model autocorrelation in the residuals. The  $\delta^{15}\text{N}$  values are irregularly spaced in  
381 time and a correlation structure that can handle the uneven spacing is needed (Pinheiro and  
382 Bates, 2000). A continuous time first-order autoregressive process (CAR(1)) is a reasonable  
383 choice; it is the continuous-time equivalent of the first-order autoregressive process (AR(1))  
384 and, simply stated, models the correlation between any two residuals as an exponentially de-  
385 creasing function of  $h(\phi^h)$ , where  $h$  is the amount of separation in time between the residuals  
386 (Pinheiro and Bates, 2000).  $h$  may be a real valued number in the CAR(1), which is how it can  
387 accommodate the irregular separation of samples in time.  $\phi$  controls how quickly the corre-  
388 lation between any two residuals declines as a function of their separation in time and is an  
389 additional parameter that will be estimated during model fitting. The model in (6) was fitted

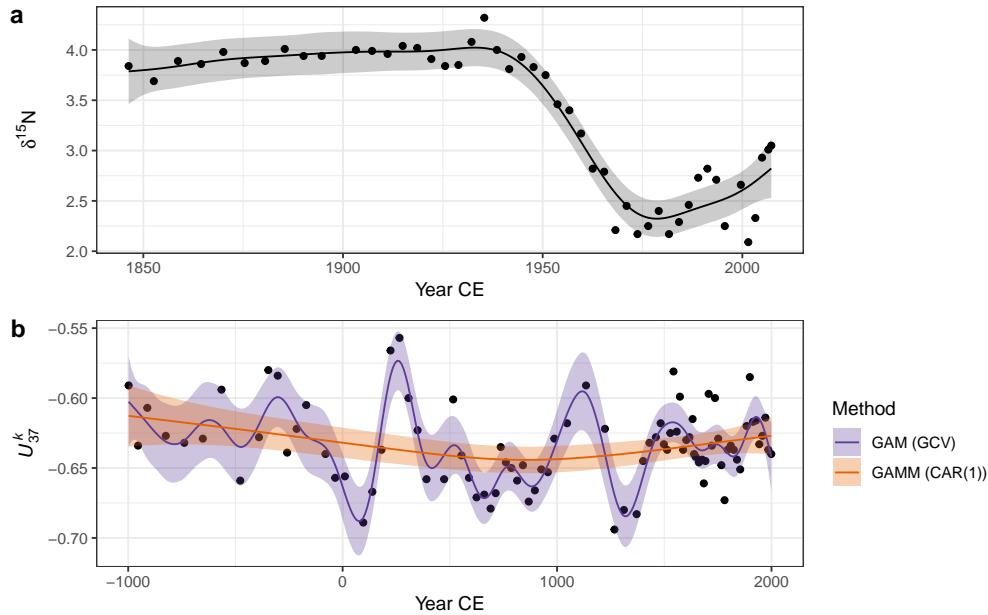


Figure 6: GAM-based trends fitted to the Small Water  $\delta^{15}\text{N}$  (a) and Braya-Sø  $U_{37}^K$  (b) time series. The shaded bands surrounding the estimated trends are approximate 95% across-the-function confidence intervals. For the  $U_{37}^K$  series, two models are shown; the orange fit is the result of a GAM with a continuous-time AR(1) process estimated using REML smoothness selection, while the blue fit is that of a simple GAM with GCV-based smoothness selection. The REML-based fit significantly oversmooths the  $U_{37}^K$  time series.

390 using the `gamm()` function (Wood, 2004) in the `mgcv` package (Wood, 2017) for R (R Core Team,  
391 2017).

392 The fitted trend is shown in Figure 6a, and well-captures the strong pattern in the data. The  
393 trend is statistically significant (estimated degrees of freedom = 7.95;  $F = 47.44$ , approximate  $p$   
394 value =  $\ll 0.0001$ ). However further analysis of the fitted model is required to answer the other  
395 questions posed earlier about the timing of change and whether features in the trend can be  
396 distinguished from random noise. I discuss these issues shortly.

## 397 4.2 Braya-Sø

398 The  $U_{37}^K$  data present a more difficult data analysis challenge than the  $\delta^{15}\text{N}$  time series because  
399 of the much more complex variation present. Fitting the same model as the Small Water ex-  
400 ample, (6), to the  $U_{37}^K$  data resulted in the unsatisfactory fit shown as the very smooth line in  
401 Figure 6b (labelled GAMM (CAR(1))). Further problems were evident with this model fit —  
402 the covariance matrix of the model was non-positive definite, a sure sign of problems with the  
403 fitted model. Refitting with a smaller basis dimension ( $k = 20$ ) for the trend term resulted in  
404 a model with a positive-definite covariance matrix for the model variance-covariance terms,  
405 but the estimated value of of the CAR(1) parameter  $\phi = 0.2$  was exceedingly uncertain (95%  
406 confidence interval 0 – 1!)

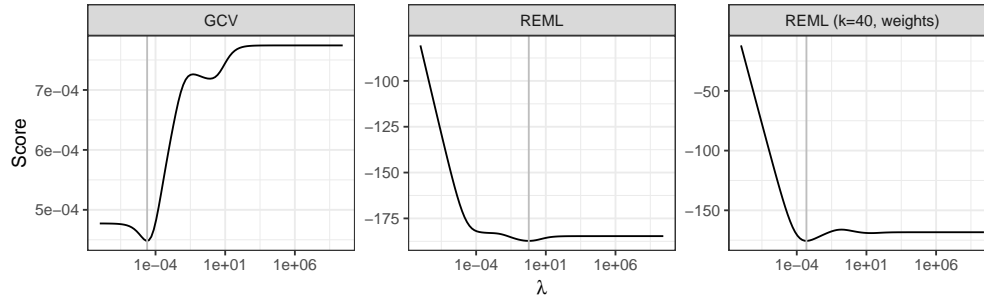


Figure 7: GCV and REML scores as a function of the smoothness parameter  $\lambda$ . From left to right, GAMs were estimated using GCV and REML smoothness selection, and REML using a basis dimension of 40 and observational weights to account for heterogeneity in the  $U_{37}^K$  times series. The selected value of  $\lambda$  for each model is indicated by the vertical grey line.

407 Fitting this model as a standard GAM with REML smoothness selection resulted in the same  
408 fitted trend as the GAM with CAR(1) errors (not shown), whilst using GCV smoothness se-  
409 lection resulted in a much more satisfactory fitted trend. There are two potential problems  
410 with the GCV-selected trend: i) GCV is sensitive to the profile of the GCV score and has been  
411 shown to under smooth data in situations where the profile is flat around the minimum GCV  
412 score, and ii) the model fitted assumes that the observations are independent, an assumption  
413 that is certainly violated in the  $U_{37}^K$  time series.

414 To investigate the first issue, the GCV and REML scores for an increasing sequence of values  
415 of the smoothness parameter ( $\lambda$ ) were evaluated for the standard GAM (equation (4)) fit to the  
416  $U_{37}^K$  time series. The resulting profiles are shown in Figure 7, with the optimal value of the  
417 parameter shown by the vertical line. The GCV score profile suggests that the potential for  
418 under smoothing identified by Reiss and Ogden (2009) is unlikely to apply here as there is a  
419 well-defined minimum in profile.

420 To understand the reason why the GAM plus CAR(1) and the simple GAM with REML smooth-  
421 ness selection performed poorly with the  $U_{37}^K$  time series we need to delve a little deeper into  
422 what is happening when we are fitting these two models.

423 The primary issue leading to poor fit is that neither model accounts for the different variance  
424 (known as (heteroscedasticity) of each observation in the  $U_{37}^K$  record. This seemingly isn't a  
425 problem for GCV which minimizes prediction error. The sediments in Braya-Sø are not an-  
426 nually laminated and therefore the core was sliced at regular depth intervals. Owing to com-  
427 paction of older sediments and variation in accumulation rates over time, each sediment slice  
428 represents a different number of "lake years". We can think of older samples as representing  
429 some average of many years of sediment deposition, whilst younger samples are representa-  
430 tive of fewer of these lake years. The average of a larger set of numbers is estimated more  
431 precisely than the average of a smaller set, all things equal. A direct result of this variable av-  
432 eraging of lake years it that some samples are more precise and therefore have lower variance  
433 than other samples and yet the model assumed that the variance was constant across samples.

434 Accounting for heteroscedasticity within the model is relatively simple via the use of observa-  
435 tional weights. The number of lake years represented by each slice is estimated by assigning a

436 date to the top and bottom of each sediment slice. The variance of each observation should be  
437 proportional to the inverse of the number of lake years each sample represents. In the `gam()`  
438 function used here, weights should be specified as the number of lake years each sample rep-  
439 resents. Other software may require the weights to be specified in a different way.

440 A secondary problem is the size of the basis dimension used for the time variable. The main  
441 user selectable option when fitting a GAM in the penalised likelihood framework of Wood  
442 (2004) is how many basis functions to use. As described above, the basis should be large  
443 enough to contain the true, but unknown, function or a close approximation to it. For GCV  
444 selection the basis used contained 29 basis functions, whilst the CAR(1) model with REML  
445 smoothness selection would only converge with a basis containing 20 functions. The size of  
446 the basis appears to be sufficient for GCV smoothness selection, but following Wood (2011)  
447 REML smoothness selection is preferred. Using the test of Pya and Wood (2016), the basis di-  
448 mension for the models with REML smoothness selection was too small. To proceed therefore,  
449 we must drop the CAR(1) term and increase the basis dimension to 39 functions (by setting  $k$   
450 = 40; I set it larger than expected because the larger basis contains a richer family of functions  
451 and the excess complexity is reduced because of the smoothness penalty.)

452 With the larger basis dimension and accounting for the non-constant variance of the observa-  
453 tions via weights, the model fitted using REML is indistinguishable from that obtained using  
454 GCV (Figure 6b). The trace of the REML score for this model shows a pronounced minimum at  
455 a much smaller value of  $\lambda$  than the original REML fit (Figure 7), indicating that a more wiggly  
456 trend provides a better fit to the Braya-Sø time series. This example illustrates that some care  
457 and understanding of the underlying principles of GAMs is required to diagnose potential is-  
458 sues with the estimated model. After standard modelling choices (size of basis to use, correct  
459 selection of response distribution and link function, etc.) are checked, it often pays to think  
460 carefully about the properties of the data and ensure that the assumptions of the model are  
461 met. Here, despite increasing the basis size, it was the failure to appreciate the magnitude of  
462 the effect of the non-constant variance that lead to the initially poor fit and the problems asso-  
463 ciated with the estimation of the CAR(1) process. I return to the issue of why the GAM plus  
464 CAR(1) model encountered problems during fitting later (see section [Residual autocorrelation  
465 and model identification](#)).

### 466 4.3 Confidence intervals and uncertainty estimation

467 If we want to ask whether either of the estimated trends is statistically interesting or proceed  
468 to identify periods of significant change, we must address the issue of uncertainty in the esti-  
469 mated model. What uncertainty is associated with the trend estimates? One way to visualise  
470 this is through a  $1 - \alpha$  confidence interval around the fitted trend, where  $\alpha$  is say 0.05 leading  
471 to a 95% interval. A 95% interval would be drawn at  $\hat{y}_t \pm (m_{1-\alpha} \times \text{SE}(\hat{y}_t))$ , with  $m_{1-\alpha} = 1.96$ , the  
472 0.95 probability quantile of a standard normal distribution<sup>1</sup>, and  $\text{SE}(\hat{y}_t)$  is the standard error of

---

<sup>1</sup>The 0.95 probability quantile of the  $t$  distribution may be used instead, which will account for estimation of  $\sigma$ , the variance of the data. However, given the number of observations, and hence residual degrees of freedom, needed to motivate fitting GAMs, differences between intervals computed using extreme quantiles of the standard normal or the  $t$  distribution will be tiny.



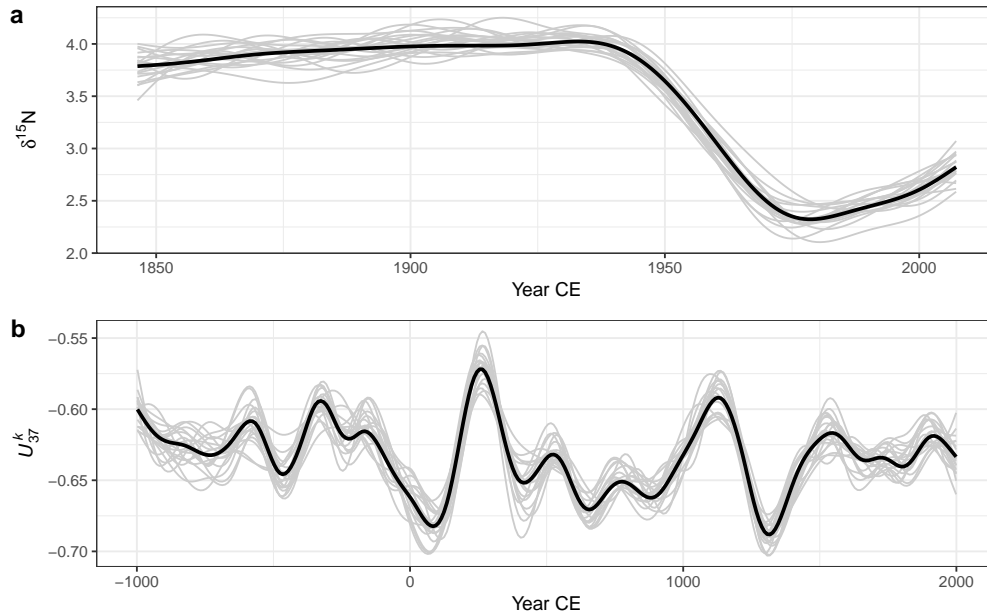


Figure 8: Estimated trends (thick black lines) and 20 random draws (grey lines) from the posterior distribution of the GAM fitted to the Small Water  $\delta^{15}\text{N}$  (a) and Braya-Sø  $U_{37}^K$  (b) time series.

473 the estimated trend at time  $x_t$ . This type of confidence interval would normally be described  
474 as *pointwise*; the coverage properties of the interval being correct for a single point on the fitted  
475 trend, but, if we were to consider additional points on the trend, the coverage would logically  
476 be lower than  $1 - \alpha$ . This is the traditional frequentist interpretation of a confidence interval.  
477 However, the GAM described here has a Bayesian interpretation (Kimeldorf and Wahba, 1970;  
478 Silverman, 1985; Wahba, 1983, 1990) and therefore the typical frequentist interpretation does  
479 not apply. Nychka (1988) investigated the properties of a confidence interval created as de-  
480 scribed above using standard errors derived from the Bayesian posterior covariance matrix for  
481 the estimated mode parameters. Such intervals have the interesting property that they have  
482 good *across-the-function* coverage when considered from a frequentist perspective. This means  
483 that, when averaged over the range of the function, the Bayesian credible intervals shown in  
484 Figure 6 have close to the expected 95% coverage. However, to achieve this some parts of the  
485 function may have more or less than 95%-coverage. Marra and Wood (2012) recently explained  
486 Nychka's (1988) surprising results and extended them to the case of generalized models (non-  
487 Gaussian responses).

488 Whilst the *across-the-function* frequentist interpretation of the Bayesian credible intervals is use-  
489 ful, it may be important to have an interval that contains the entirety of the true function with  
490 some state probability  $(1 - \alpha)$ . Such an interval is known as a *simultaneous* interval. A  $(1 - \alpha)100\%$   
491 simultaneous confidence interval contains *in their entirety*  $1 - \alpha$  of all random draws from the  
492 posterior distribution of the fitted model.

493 Fitting a GAM involves finding estimates for coefficients of the basis functions. Together, these  
494 coefficients are distributed multivariate normal with mean vector and covariance matrix spec-  
495 ified by the model estimates of the coefficients and their covariances respectively. Random

496 draws from this distribution can be taken, where each random draw represents a new trend  
497 that is consistent with the fitted trend but also reflects the uncertainty in the estimated trend.  
498 This process is known as *posterior simulation*.

499 Figure 8 shows 20 random draws from the posterior distributions of the GAMs fitted to the  
500 Small Water and Braya-Sø data sets. In the early period of the  $\delta^{15}\text{N}$  time series many of the pos-  
501 terior simulations exhibit short periods of increasing and decreasing trend, balancing out to  
502 the relatively flat trend estimated by the GAM (Fig. 8a). Reflecting this uncertainty, we might  
503 expect relatively wide simultaneous intervals during this period in order to contain the vast  
504 majority of the simulated trends. Conversely, the decreasing  $\delta^{15}\text{N}$  trend starting at  $\sim 1945$  is  
505 consistently reproduced in the posterior simulations, suggesting that this feature of the time  
506 series is both real and statistically significant, and that the rate of change in  $\delta^{15}\text{N}$  is relatively  
507 precisely estimated. We see a similar pattern in Figure 8b for the Braya-Sø record; the large  
508 peak in  $U_{37}^K$  at  $\sim 250\text{CE}$  and the strong decline at  $\sim 1200\text{CE}$  are well defined in the posterior  
509 simulations, whereas most of the localised trends that are smaller magnitude changes in  $y_t$   
510 are associated with posterior simulations that are less well constrained with the ends of the  
511 record in particular showing considerable variation in the strength, timing, and even sign of  
512 simulated trends, reflecting the greater uncertainty in estimated trend during these periods.  
513 For the random draws illustrated in Figure 8, a  $(1 - \alpha)100\%$  simultaneous interval should con-  
514 tain the entire function for on average 19 of the 20 draws.

515 There are a number of ways in which a simultaneous interval can be computed. Here I follow  
516 the simulation approach described by Ruppert et al. (2003) and present only the basic detail; a  
517 fuller description is contained in Appendix 1. The general idea is that if we want to create an  
518 interval that contains the whole of the true function with  $1 - \alpha$  probability, we need to increase  
519 the standard Bayesian credible interval by some amount. We could simulate a large number  
520 of functions from the posterior distribution of the model and then search for the value of  $m_{1-\alpha}$   
521 that when multiplied by  $\text{SE}(\hat{f}(x_t))$  yielded an interval that contained the whole function for  
522  $(1 - \alpha) 100\%$  of the functions simulated. In practice, the simulation method of Ruppert et al.  
523 (2003) does not involve a direct search, but yields the critical value  $m_{1-\alpha}$  required.

524 Simultaneous intervals computed using the method described are show in Figure 9 alongside  
525 the *across-the-function* confidence intervals for the trends fitted to both example data sets. As  
526 expected, the simultaneous interval is somewhat wider than the *across-the-function* interval.  
527 The critical value  $m_{1-\alpha}$  for the simultaneous interval of the estimated trend in  $\delta^{15}\text{N}$  is 3.07,  
528 whilst the same value for the  $U_{37}^K$  series is 3.43, leading to intervals that are approximately  
529  $\pm 50\%$  and  $\pm 75\%$  wider than the equivalent across-the-function intervals.

#### 530 4.4 Identifying periods change

531 In the simple linear trend model (1) whether the estimated trend constitutes evidence for or  
532 against a null hypothesis of no change rests on how large the estimated rate of change in  $y_t$   
533 is ( $\hat{\beta}_1$ ) relative to its uncertainty. This is summarised in the  $t$  statistic. As the rate of change  
534 in  $y_t$  is constant over the fitted trend — there is only a single slope for the fitted trend  $\hat{\beta}_1$  — if  
535 the  $t$  statistic of the test that  $\hat{\beta}_1 = 0$  is unusually extreme this would be evidence against the  
536 null hypothesis of no change. Importantly, this applies to the whole time series as the linear

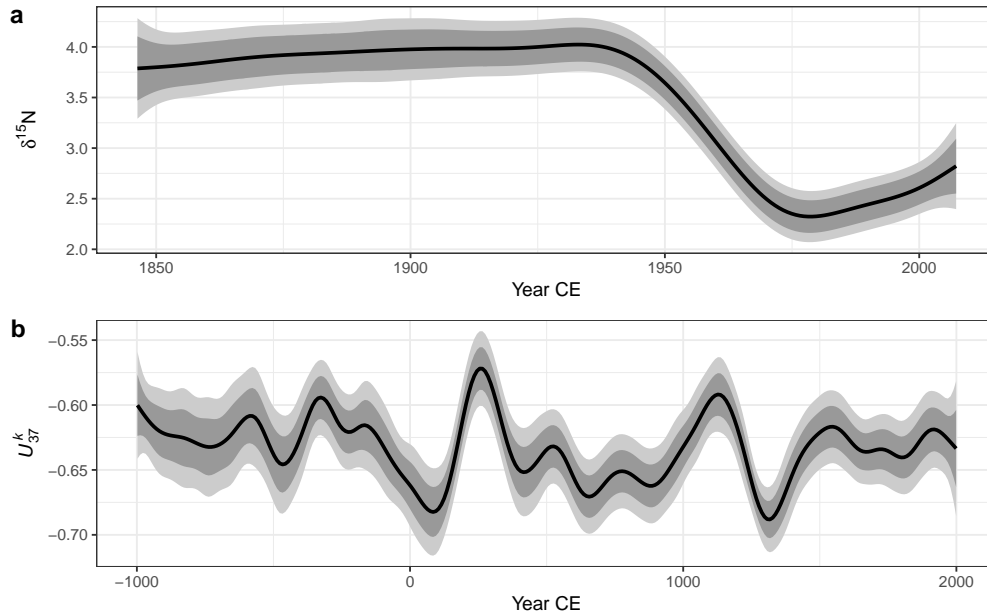


Figure 9: 95% simultaneous confidence intervals (light grey bands) and across-the-function confidence intervals (dark grey bands) on the estimated trends (black lines) for the Small Water  $\delta^{15}\text{N}$  (a) and Braya-Sø  $U_{37}^K$  (b) time series.

537 model implies a constant rate of change throughout. More formally, the estimate  $\hat{\beta}_1$  is the first  
538 derivative of the fitted trend.

539 In the GAM, the fitted trend need not be linear; the slope of the trend is potentially different  
540 at every point in the time series. As such we might reasonably ask *where* in the series the  
541 response  $y_t$  is changing, if at all? Mirroring the linear model we can answer this question by  
542 determining whether or not the first derivative at any time point  $x_t$  of the fitted trend at any  
543 time point is consistent with a null hypothesis of no change. We want to know whether or not  
544 the first derivative is indistinguishable from a value of 0 — no trend — given the uncertainty  
545 in the estimate of the derivative.

546 Derivatives of the fitted spline are not easily available analytically, but they can be estimated  
547 using the method of finite differences. Two values of the estimated trend, separated by a very  
548 small time-shift ( $\Delta_t$ ), are predicted from the model; the difference between the estimated values  
549 for the two time points is an approximation of the true first derivative of the trend. As  $\Delta_t \rightarrow 0$   
550 the approximation becomes increasingly accurate. In practice, the first derivative of the fitted  
551 trend is evaluated using finite differences at a large number of points in the time series. An  
552 approximate  $(1 - \alpha)100\%$  pointwise confidence interval can be calculated for the derivative  
553 estimates using standard theory (i.e.  $\pm 1.96 \times \text{SE}(\hat{y}_t)$  for a 85% interval) and the covariance matrix  
554 of the spline coefficients. A  $(1 - \alpha)100\%$  simultaneous interval for the derivatives can also be  
555 computed using the method described [earlier](#). Periods of significant change are identified as  
556 those time points where the (simultaneous) confidence interval on the first derivative does not  
557 include zero.

558 Figure 10 shows the estimated first derivative of the fitted trend in the Small Water (10a) and

559 Braya-Sø (10b) time series. Although the estimated trend suggests a slight increase in  $\delta^{15}\text{N}$   
560 from the start of the record to  $\sim 1940$ , the estimated trend is sufficiently uncertain that the si-  
561 multaneous interval on the first derivative includes 0 throughout. We can understand why this  
562 is so by looking at the posterior simulations in Figure 8a; there is considerable variation in the  
563 shape of the simulated trends throughout this period. From  $\sim 1925$  the derivative of the trend  
564 becomes negative, however it is not until  $\sim 1940$  that the simultaneous interval doesn't include  
565 0. At this point we have evidence to reject the null hypothesis of no change. This time point  
566 may be taken as the first evidence for change in  $\delta^{15}\text{N}$  in the Small Water core. The simultane-  
567 ous interval on the first derivative of the trend in  $\delta^{15}\text{N}$  is bounded away from 0 between  $\sim 1940$   
568 and  $\sim 1975$ , covering the major decline in values evident in the observations. The simultaneous  
569 interval includes 0 from  $\sim 1975$  onward, suggesting that, whilst quite pronounced, the recent  
570 increase in  $\delta^{15}\text{N}$  is not statistically significant. To determine whether or not the recent increase  
571 is real, we would require considerably more samples with which to (hopefully) more-precisely  
572 estimate the trend during this period. Alternatively, we might just have to wait until sufficient  
573 additional sedimentation has occurred to warrant recoring Small Water and reestimating the  
574 trend in  $\delta^{15}\text{N}$ .

575 The estimated trend at Braya-Sø exhibited a number of oscillations in  $U_{37}^K$ . As we saw previ-  
576 ously in Figures 8b and 9b, many of these are subject to significant uncertainty and it is impor-  
577 tant therefore to discern which, if any, of the oscillations in the response can be identified given  
578 the model uncertainty. In Figure 10b only two features of the estimated trend are considered  
579 significant based on the derivatives of the smooth; one centred on  $\sim 250\text{CE}$  and a second at  
580  $\sim 1150\text{CE}$ . In both these periods, the simultaneous interval for the first derivative of the trend  
581 does not include zero. In the first case we detect the large peak and subsequent decline in  
582  $U_{37}^K$  at  $\sim 250\text{CE}$ , whilst at  $\sim 1150\text{CE}$  the large trough is identified, but not the increasing trend  
583 immediately prior to this excursion to lower  $U_{37}^K$ . Recall that these intervals are simultaneous  
584 in nature, strongly guarding against false positives, and as such we can be confident in the  
585 estimation of these two features, whilst care must be taken to not over-interpret the remaining  
586 variations in the estimated trend.

## 587 4.5 Residual autocorrelation and model identification

588 The GAM fitted to the  $\delta^{15}\text{N}$  time series contained a CAR(1) process to model residual temporal  
589 autocorrelation in the residuals. The estimated magnitude of the autocorrelation is given by  
590 the parameter  $\phi$ . The estimated value of  $\phi$  for the  $\delta^{15}\text{N}$  series is 0.6 with 95% confidence in-  
591 terval 0.28–0.85, indicating moderate to strong residual autocorrelation about the fitted trend.  
592 The correlation function is an exponentially decreasing function of temporal separation ( $\Delta_t$ ),  
593 and whilst observations that are a few years apart are quite strongly dependent on one an-  
594 other, this dependence drops off rapidly as  $\Delta_t$  increases and is effectively zero when samples  
595 are separated by a decade or more (Figure 11).

596 Failure to account for the dependencies in the  $\delta^{15}\text{N}$  time series could lead to the estimation  
597 of a more wiggly trend than the one shown in Figure 6a which would negatively impact the  
598 confidence placed on the inferences we might draw from the fitted model. Importantly, fail-  
599 ing to account for the strong dependency in the residuals would lead to smaller uncertainties

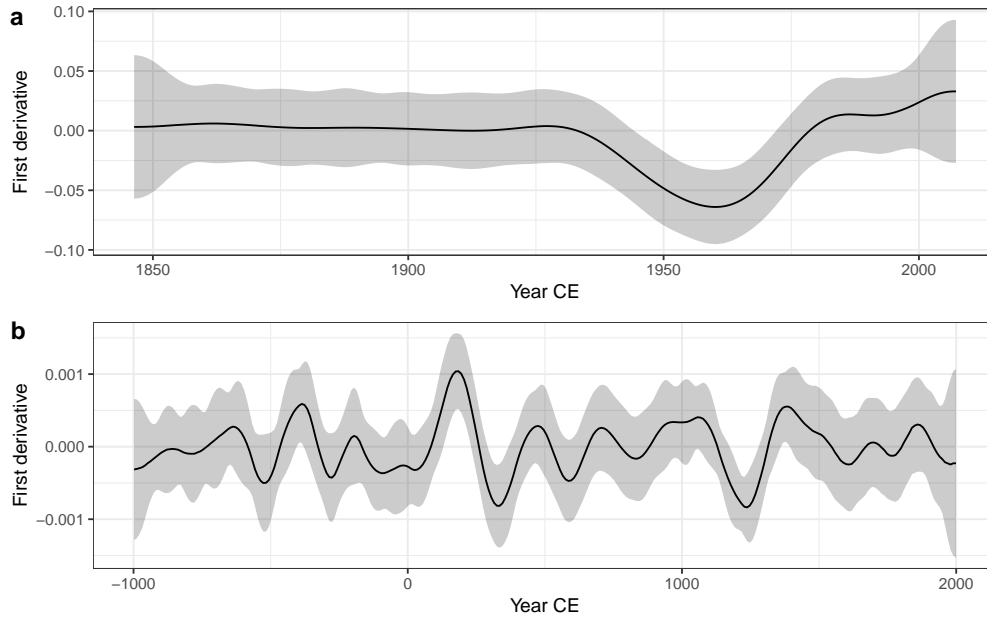


Figure 10: Estimated first derivatives (black lines) and 95% simultaneous confidence intervals of the GAM trends fitted to the Small Water  $\delta^{15}\text{N}$  (a) and Braya-Sø  $U_{37}^K$  (b) time series. Where the simultaneous interval does not include 0, the models detect significant temporal change in the response.

600 in the estimated spline coefficients, which would propagate through to narrower confidence  
 601 intervals on the fitted trend and on the first derivatives, and ultimately to the identification of  
 602 significant periods of change. The end result would be a tendency toward anti-conservative  
 603 identification of periods of change; the coverage probability would be lower than the anticipi-  
 604 pated  $1 - \alpha$ , leading to a greater chance of false positive results.

605 Problems estimating the GAM plus CAR(1) model were encountered when this was fitted to  
 606 the  $U_{37}^K$  time series; including both a smooth trend in the mean  $U_{37}^K$  and a CAR(1) process in  
 607 the residuals lead to an unidentifiable model. What makes a model with a spline-based trend  
 608 and an autocorrelation process like the CAR(1) potentially unidentifiable?

609 Consider again the basic GAM for a smooth trend, (3). In that equation the correlation ma-  
 610 trix  $\Lambda$  was omitted for the sake of simplicity. As I did in (6), I reintroduce it and restate the  
 611 distributional assumptions of this model

$$y_t = \beta_0 + f(x_t) + \varepsilon_t, \quad \varepsilon \sim (0, \Lambda\sigma^2) \quad (7)$$

612 In the basic GAM,  $\Lambda \equiv \mathbf{I}$  is an identity matrix, a matrix with 1s on the diagonal and 0s elsewhere

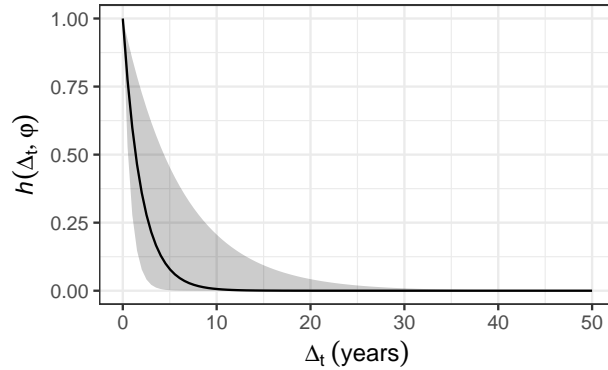


Figure 11: Estimated CAR(1) process from the GAM fitted to the Small Water  $\delta^{15}\text{N}$  time series.  $h(\Delta_t, \phi)$  is the correlation between residuals separated by  $\Delta_t$  years, where  $\hat{\phi} = 0.6$ . The shaded band is a 95% pointwise confidence interval on the estimated correlation  $h$ .

$$\begin{bmatrix} 1 & 0 & 0 & \dots & 0 \\ 0 & 1 & 0 & \dots & 0 \\ 0 & 0 & 1 & \dots & 0 \\ \vdots & \vdots & \vdots & \ddots & \vdots \\ 0 & 0 & 0 & \dots & 1 \end{bmatrix},$$

613 which is where the independence assumption of the model comes from; a model residual is  
 614 perfectly correlated with itself (the 1s on the diagonal), but uncorrelated with any other resid-  
 615 ual (the off-diagonal 0s). In the GAM plus CAR(1) model, an alternative correlation function  
 616 for  $\Lambda$  was used — the CAR(1) with correlation parameter  $\phi$ . Fahrmeir and Kneib (2008) show  
 617 that where the stochastic structure of  $f$  and  $\Lambda$  approach one another, i.e. where we have a  
 618 potentially wiggly trend or strong autocorrelation as  $\phi \rightarrow 1$ , the two processes can quickly  
 619 become unidentifiable (see also Fahrmeir et al., 2013). By unidentifiable, we mean that it be-  
 620 comes increasingly difficult to distinguish between a wiggly trend or strong autocorrelation  
 621 because these two processes are very similar to one another in appearance. This leads to model  
 622 estimation problems of the sort encountered with fitting the GAM plus CAR(1) model to the  
 623 Braya-sø  $U_{37}^K$  series.

624 Why might this be so? Autocorrelation is the tendency for a large (small) value of  $y_t$  at time  $x_t$   
 625 to be followed by a likewise large (small) value at time  $x_{t+1}$ . This leads to runs of values that  
 626 are consistently greater (less) than the overall mean. Short runs would indicate weaker auto-  
 627 correlation whilst longer runs are associated with stronger autocorrelation, and long runs of  
 628 values greater (less) than the mean would be evident as non-linear trends in the time series. As  
 629 a result, a wiggly trend and an autocorrelation function with large  $\phi$  are two ways to describe  
 630 the same pattern of values in a time series, and, without any further information to constrain  
 631 either of these, the model is unable to distinguish both components uniquely.

632 Situations where it may be possible to uniquely identify separate wiggly trends and autocor-  
 633 relation are exemplified by the Small Water  $\delta^{15}\text{N}$  time series. The non-linear trend and the  
 634 autocorrelation operate at very different scales; the trend represents decadal-scale variation in

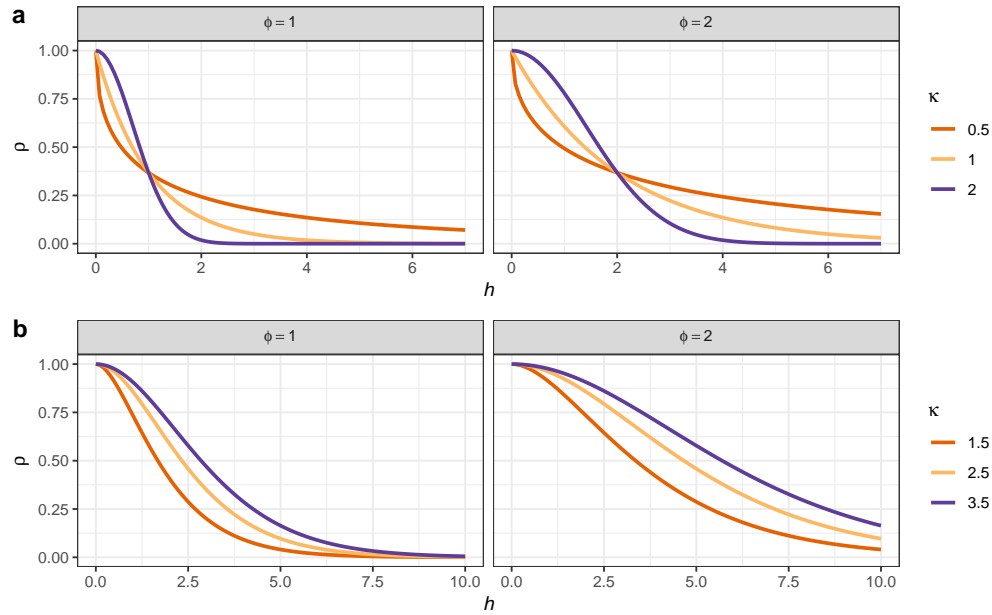


Figure 12: Power exponential (a) and Matérn (b) correlation functions for observation separation distance  $h$ . Two values of the effective range parameter ( $\phi$ ) are shown for each function. For the power exponential function,  $\kappa$  is the power in the power exponential function. For the Matérn correlation function,  $\kappa$  distinguishes the member of the Matérn family.

635 mean  $\delta^{15}\text{N}$ , whilst the CAR(1) process represents the much smaller-scale tendency for values  
 636 of the response to be followed in time by similar values. That such a pattern is observed in  
 637 the Small Water core is the result of the high resolution of the sampling in time relative to the  
 638 long-term trend. In contrast, the Braya-Sø record is sampled at far lower resolution relative  
 639 to the fluctuations in the mean response, and consequently the data do not contain sufficient  
 640 information to separate trend and autocorrelation.

## 641 4.6 Gaussian process smooths

642 In the world of machine learning, Gaussian processes (Golding and Purse, 2016; Rasmussen  
 643 and Williams, 2006) are a widely-used method for fitting smooth non-parametric regression  
 644 models. A Gaussian process is a distribution over all possible smooth functions  $f(x)$ . In the  
 645 field of spatial statistics, Gaussian processes are known by the name *kriging*.

646 With a Gaussian process we are interested in fitting a smooth temporal trend by modelling  
 647 the way the correlation between pairs of observations varies as a function of the distance,  $h$ , in  
 648 time that separates the observations. The correlation between pairs of observations decreases  
 649 with increasing separation, which is modelled using a correlation function,  $c(h)$ .

650 Several functions can be used to represent  $c(h)$ . Two common ones are the power exponential  
 651 function and the Matérn family of correlation functions. The power exponential function at  
 652 separation distance  $h$  is

$$c(h) = \exp\{(-h/\phi)^\kappa\}$$

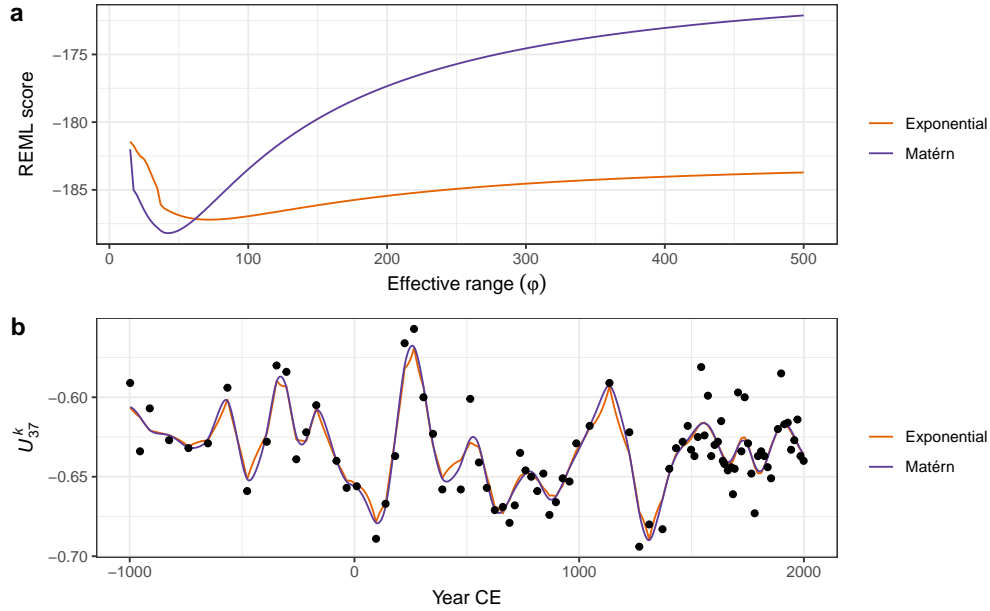


Figure 13: Gaussian process smooths fitted to the  $U_{37}^k$  time series. REML score traces for GAMs fitted using power exponential ( $\kappa = 1$ ) or Matérn ( $\kappa = 1.5$ ) correlation functions as a function of the effective range parameter ( $\phi$ ) are shown (a). The optimal model for each function is that with the lowest REML score. b) shows the resulting trends estimated using the respective correlation function with the value of  $\phi$  set to the optimal value.

653 where  $0 < \kappa \leq 2$ . The Matérn correlation function is actually a family of functions with closed-  
 654 forms only available for a subset of the family, distinguished by  $\kappa$ . When  $\kappa = 1.5$ , the Matérn  
 655 correlation function is

$$c(h) = (1 + h/\phi) \exp(-h/\phi)$$

656 whilst for  $\kappa = 2.5$  it is

$$c(h) = \{1 + h/\phi + (h/\phi)^2/3\} \exp(-h/\phi)$$

657 and for  $\kappa = 3.5$

$$c(h) = \{1 + h/\phi + 2(h/\phi)^2/5 + (h/\phi)^3/15\} \exp(-h/\phi).$$

658 In all cases,  $\phi$  is the effective range parameter, which sets the distance beyond which the cor-  
 659 relation function is effectively zero.

660 Figure 12 shows examples of two different correlation functions; the *power exponential* (Fig-  
 661 ure 12a), and the Matérn (Figure 12b) correlation functions. These functions are smooth and  
 662 monotonic-decreasing, meaning that the value of the correlation function decreases with in-  
 663 creasing separation ( $h$ ). When  $h = 0$ , the correlation is equal to 1 ( $c(0) = 1$ ); two samples taken  
 664 at exactly the same time point are perfectly correlated. As  $h \rightarrow \infty$ , the correlation tends to zero  
 665 ( $c(h) \rightarrow 0$ ); two samples separated by a large amount of time tend to be uncorrelated. Often  
 666 we are interested in learning how large the separation in time needs to be before, on average,  
 667 a pair of observations is effectively uncorrelated (i.e. where  $c(h)$  is sufficiently close to zero).



668 Gaussian processes and GAMs share many similarities and we can fit a Gaussian process using  
669 the techniques already described above for splines (Handcock et al., 1994; Kammann and  
670 Wand, 2003). It can be shown (e.g. Fahrmeir et al., 2013) that the Gaussian process model has  
671 the same penalised likelihood form as the GAM that we discussed earlier; the observations are  
672 the knots of the smoother and each has a basis function in the form of a correlation function.  
673 The equivalence is only true if the basis functions do not depend on any other parameters of  
674 the model, which is only achievable if the value of  $\phi$  is fixed and known (Fahrmeir et al., 2013).  
675 In general, however, we would like to estimate  $\phi$  as part of model fitting. To achieve this we  
676 can maximise the profile likelihood or score statistic of the model over a range of values of  
677  $\phi$  (Wood, 2017, 362–363). This involves proposing a value of  $\phi$  for the effective range of the  
678 correlation function and then estimating the resulting GAM by minimising the penalised log-  
679 likelihood conditional upon this value of  $\phi$  and repeating for a range of values for  $\phi$ . The model,  
680 and its corresponding value of  $\phi$ , with lowest penalised log-likelihood or score statistic is then  
681 retained as the estimated GAM. Figure 13a shows the REML score for models estimated using  
682 a Gaussian process smooth with a Matérn correlation function ( $\kappa = 1.5$ ) for a sequence of values  
683 of  $\phi$  between 15 and 1000 years. There is a clear minimum around 40 years separation, with  
684 the minimum REML score being observed at  $\phi = 41.81$ ). Also shown are the REML scores for  
685 models using the power exponential function ( $\kappa = 1$ ) with the minimum score observed at a  
686 somewhat higher effective range of  $\phi = 71.06$ .

687 Figure 13b shows the estimated trends for the  $U_{37}^K$  time series using Gaussian process smooths  
688 with exponential and Matérn correlations functions, both using  $\phi$  values at their respective  
689 optimal value as assessed using the REML score. The estimated trends are very similar to  
690 one another, although there is a noticeable difference in behaviour, with the power exponential  
691 ( $\kappa = 1$ ) version being noticeably less-smooth than the Matérn version. This difference is  
692 attributable to the shapes of the respective correlation functions; the Matérn approaches a cor-  
693 relation of 1 smoothly as  $h$  approaches 0, whilst the power exponential with  $\kappa = 1$  approaches  
694 a correlation of 1 increasingly quickly with decreasing  $h$ . The power exponential with  $\kappa =$   
695 2, like the Matérn, approaches  $\phi = 1$  smoothly, and consequently the trend estimated using  
696 this correlation function is qualitatively similar to that estimated using the Matérn correlation  
697 function.

## 698 4.7 Adaptive smoothing

699 Each of the spline types that I have discussed so far shares a common feature; the degree of  
700 wiggleness over the time series is fixed due to the use of a single smoothness parameter,  $\lambda$ . The  
701 definition of wiggleness, as the integrated squared second derivative of the spline, ensures that  
702 the fitted smoother does not jump about wildly. This assumes that the data themselves are well  
703 described by a smoothly varying trend. If we anticipate abrupt change or step-like responses to  
704 environmental forcing this underlying assumption of the GAM would suggest that the method  
705 is ill-suited to modelling palaeo time series in which such features are evident or expected.

706 While there is not much we can do within the GAM framework to model a series that contains  
707 both smooth trends and step-like responses, an adaptive smoother can help address problems  
708 where the time series consists of periods of rapid change in the mean combined with periods

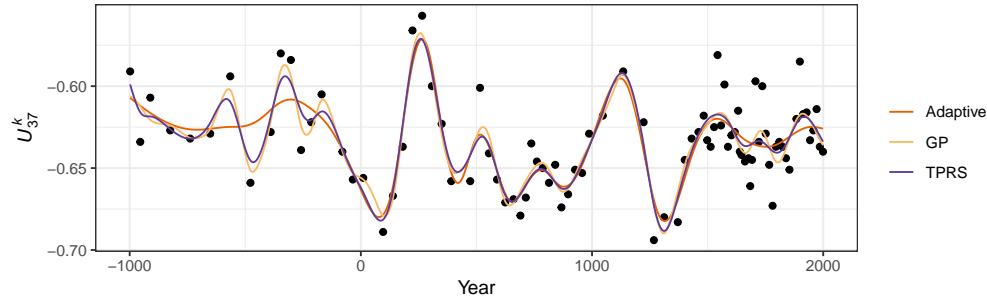


Figure 14: Comparison of trends estimated using i) adaptive smooth, ii) Gaussian process, and iii) thin plate regression spline bases for the  $U_{37}^k$  time series.

709 of complacency or relatively little change. As suggested by their name, adaptive smoothers  
710 can adjust to changes in the wiggleness of the time series. This adaptive behaviour is achieved  
711 by making the smoothness parameter  $\lambda$  itself depend smoothly on  $x_t$  (Ruppert et al., 2003,  
712 17; Wood, 2017, 5.3.5); in other words, the adaptive smoother allows the wiggleness of the  
713 estimated trend to vary smoothly over time. Whilst this allows the estimated trend to adapt  
714 to periods of rapid change in the response, adaptive smoothers make significant demands on  
715 the data (Wood, 2017, 5.3.5); if we used  $m$  smoothness penalties to allow the wiggleness to  
716 vary over a time series, it would be like estimating  $m$  separate smooths from chunks of the  
717 original series each of length  $n/m$ . In a practical sense, this limits the use of adaptive splines  
718 in palaeoecology to proxies that are readily enumerated, such as the biogeochemical proxies  
719 used in the two example data sets.

720 Figure 14 compares trends for the Braya-Sø time series estimated using GAMs with the three  
721 main types of spline discussed; i) TPRS, ii) Gaussian process smooths, and iii) an adaptive  
722 smoother using 45 basis functions and 5 smoothing parameters. There is a clear difference  
723 in the behaviour of the adaptive and non-adaptive smoothers for the first 1000 years of the  
724 record, with the adaptive smooth exhibiting much less variation compared with either the  
725 TPRS or Gaussian process splines. Over the remaining two thirds of the series, there is much  
726 closer agreement in the three smooths.

727 The behaviour of the TPRS and Gaussian process splines for these data is the result of requiring  
728 a large amount of wiggleness (a small  $\lambda$ ) to adapt to the large oscillations in  $U_{37}^k$  present around  
729 year 250CE and again at ~900–1500CE. This large degree of wiggleness allows the splines to  
730 potentially over-fit individual data points much earlier in the record. Because the adaptive  
731 smoother, in contrast, can adapt to these periods of rapid change in the response it is much  
732 less susceptible to this “chasing” behaviour — we don’t need to waste effective degrees of  
733 freedom in periods with little or no change just to be able to fit the data well when there is a  
734 lot of change.

735 This potential for over-fitting in such situations is undesirable, yet if we recall Figure 10 and  
736 the discussion around the use of the first derivative to identify periods of significant change,  
737 we would not interpret the oscillations in the early part of the  $U_{37}^k$  record as being statistically  
738 significant. Owing to the paucity of data in this part of the series the trends fitted using the  
739 non-adaptive smoothers are subject to such a large degree of uncertainty that the alternative

740 of no trend through the first 1000 years of the record is also a plausible explanation of the data.  
741 The trend estimated using the adaptive smooth reflects this. Therefore, should we conclude  
742 that there is no trend in  $U_{37}^K$  and thence climate in this period? I believe that to be too-strong a  
743 statement; those oscillations in  $U_{37}^K$  may be real responses to climate forcing but we may simply  
744 lack the statistical power to distinguish them from the null hypothesis of no trend through  
745 this period. The adaptive smoother is only adjusting to the data available to it; just because  
746 it does not detect a trend during this period does not lend itself to an interpretation of stable  
747 climate forcing or complacency in the lake's response to forcing (although that is a justifiable  
748 interpretation of the result). If there were particular interest in the climate of this particular  
749 period we might take from the Braya-Sø record that there is potential early variation due to  
750 climate forcing, but that additional data from this or other sites is required before any definitive  
751 conclusion can be drawn.

## 752 4.8 Accounting for age model uncertainty

753 Thus far, the trend models that I have described and illustrated assumed that the time co-  
754 variate ( $x_t$ ) was fixed and known. In both examples, and generally for most palaeoecological  
755 records, this assumption is violated. Unless the record is annually laminated, assigning an  
756 age to a sediment interval requires the development of an age model from observations of the  
757 relationship between depth down the sediment core and estimates of the age of the sample  
758 arrived at using any of a number of techniques, for example  $^{210}\text{Pb}$  or  $^{14}\text{C}$  radiometric dating.  
759 This age-depth relationship is itself uncertain, usually being derived from a mathematical or  
760 statistical model applied to point age estimates (e.g. Blaauw and Heegaard, 2012). Incorporat-  
761 ing this additional component of uncertainty complicates the estimation of statistical models  
762 from palaeoenvironmental data. In this section I illustrate a simulation based approach to  
763 quantify and account for age-model uncertainty as part of the trend estimation using a GAM  
764 (see Anchukaitis and Tierney (2013) for a similar, non-GAM related idea).

765 Figure 15a shows the estimated dates (in Years CE) for 12 levels in the Small Water core dated  
766 using  $^{210}\text{Pb}$ . The vertical bars show the estimated age uncertainty of each level. The solid line  
767 through the data points is an additive model fitted to the observations, with prior weights  
768 given by the estimated age uncertainties. The fitted age-depth model is constrained to be  
769 monotonically decreasing with increasing depth, following the method of (Pya and Wood,  
770 2015) using the *scam* package (Pya, 2017). Also shown are 25 simulations from the posterior  
771 distribution of the monotonically-constrained GAM. Each simulation from the posterior dis-  
772 tribution of the age-model is itself a potential age-depth model, which can be used to assign  
773 dates to the Small Water core. The trend model in (4) can be fitted to the  $\delta^{15}\text{N}$  data using these  
774 new dates as  $x_t$ , and the whole process repeated for a large number of simulations from the  
775 age model.

776 Figure 15b shows the trend in  $\delta^{15}\text{N}$  for the observed age-depth model, plus trends estimated  
777 via the same model using 100 draws from the posterior distribution of the age model. In this  
778 case, the age-depth model is relatively simple with little variation in the posterior draws, re-  
779 sulting in trends that match closely that obtained from the estimated age-depth relationship.  
780 Even so, this additional uncertainty suggests that the timing of the decline in  $\delta^{15}\text{N}$  covers the

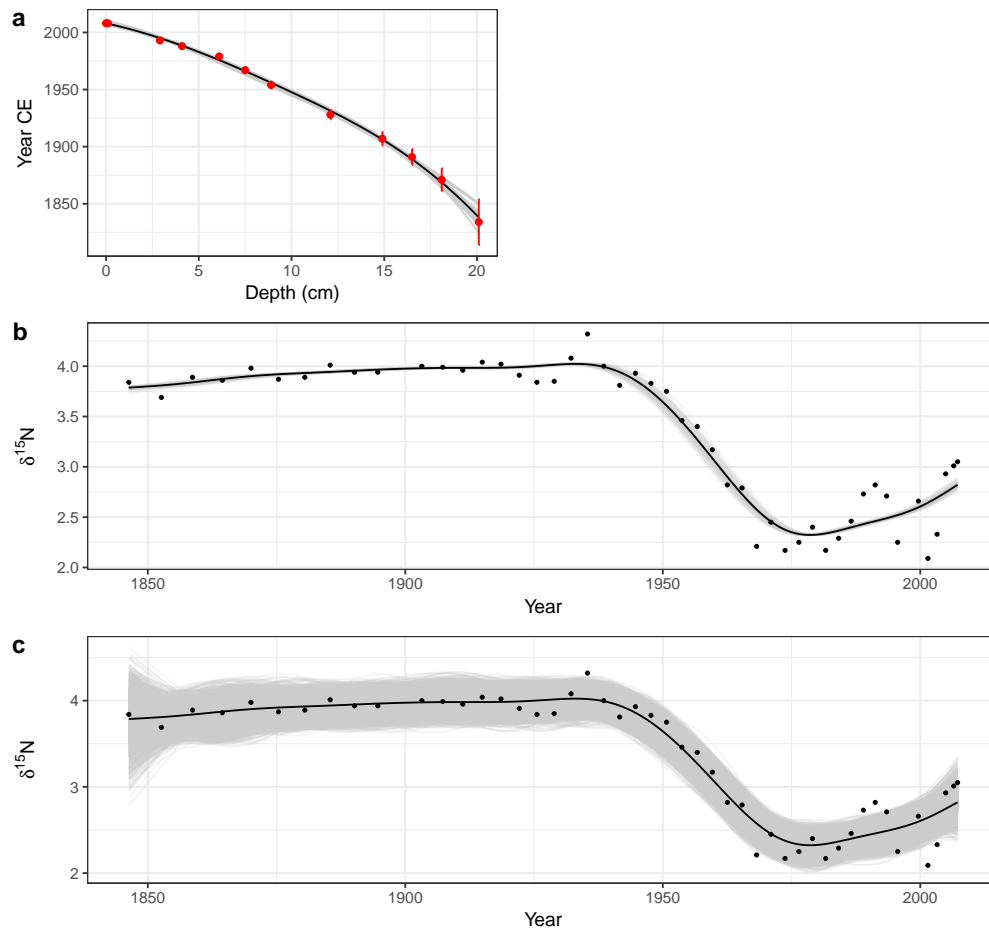


Figure 15: Accounting for uncertainty in age estimates whilst fitting a smooth trend to the Small Water  $\delta^{15}\text{N}$  time series. (a) Estimated age model using a monotonically-constrained spline fitted to  $^{210}\text{Pb}$  inferred ages for selected depths in the sediment core (red points). The uncertainty in the  $^{210}\text{Pb}$  inferred age is shown by the red vertical bars. The fitted age model is illustrated by the solid black line. The faint grey lines are 25 random draws from the posterior distribution of the monotonically constrained GAM. The effect of age uncertainty on trend estimation is shown in b); for 100 simulations from the posterior distribution of the age model in a) a trend was estimated using a GAM with a thin plate regression spline basis and a CAR(1) process in the residuals. These trends are shown as grey lines. The combined effect of age model and fitted GAM uncertainty on the trends for the  $\delta^{15}\text{N}$  time series is shown in c). The grey lines in c) are based on 50 random draws from the model posterior distribution for each of the 100 trends shown in b). For both b) and c) the black line shows the trend estimated assuming the ages of each sediment sample are known and fixed.

781 interval ~1935–1945.

782 The uncertainty in the trend estimates illustrated in Figure 15b only reflects the variation in  
783 trends fitted to the uncertain dates of the sediment samples. To fully visualise the uncertainty  
784 in the trend estimates, incorporating both age model uncertainty *and* uncertainty in the esti-  
785 mated model coefficients themselves, 50 simulations from the posterior distribution of each  
786 of the 100 estimated trends shown in Figure 15b were performed, resulting in 5,000 trend esti-  
787 mates for the  $\delta^{15}\text{N}$  series. These are shown in Figure 15c, where the two obvious changes over  
788 the same simulations without accounting for uncertainty in  $x_t$  (Figure 8a) are that the uncer-  
789 tainty band traced out by the simulations is approximately 50% wider and, not surprisingly,  
790 the uncertainty in the estimated trend is most pronounced in the least accurately-dated sec-  
791 tion of the core. Despite this additional uncertainty however, the main result holds; a marked  
792 decline of  $\sim 1.5\text{‰}$  that occurred between approximately 1930 and 1945, with mild evidence of  
793 a small increase in  $\delta^{15}\text{N}$  post 2000 CE.

#### 794 4.9 Multivariate data

795 A large proportion of the palaeoenvironmental data generated today is multivariate in nature  
796 and yet the two examples used to illustrate GAMs were univariate. Can the approach de-  
797 scribed here be used for multivariate data? Yes, and no. With one main exception it is not  
798 possible to directly apply the GAM methodology described here to multivariate abundance  
799 data, where the aim is to model all species at once. The *mgcv* software, for example, is not able  
800 to estimate the penalized GAM for multiple non-Gaussian responses. The exception is for a  
801 small number of correlated Gaussian responses; these could be modelled as being distributed  
802 multivariate normal conditional upon the covariates. Such a model would estimate the ex-  
803 pected values of each response and the correlations between them. For example, we could  
804 jointly model  $\delta^{15}\text{N}$  and  $\delta^{13}\text{C}$  series using this approach.

805 Formal multivariate versions of GLM or GAMs are currently an important area of research  
806 within ecology (see Warton et al. (2015) for a recent review), where they go by the name joint  
807 species distribution models (JSDMs). Whilst undoubtedly powerful, our knowledge regard-  
808 ing JSDMs and their availability in software are still in their relative infancy and they require  
809 considerable expertise to implement. As such, JSDMs are currently beyond the reach of most  
810 palaeoecologists. Despite this, we should be watching JSDM research as developments are  
811 ongoing and a degree of method maturation occurring.

812 One currently available avenue for fitting a multivariate GAM is via regularized sandwich  
813 estimators and GLMs (Warton, 2011), which involves fitting separate GLMs (or GAMs) to  
814 each response variable and subsequently using resampling-based hypothesis tests to deter-  
815 mine which covariates are related to variation at the community level and for individual taxa  
816 (Wang et al., 2012; Warton, 2011; Warton et al., 2012). The *mvabund* package (Wang et al., 2012)  
817 implements this approach within R and can use *mgcv* to fit GAMs to each species.

818 A pragmatic although inelegant approach that has been used to estimate trends in multivariate  
819 palaeoecological data is to first summarise the response data using an unconstrained ordina-  
820 tion via a PCA, CA, or principal curve and then fit separate GAM models to the site (sample)  
821 scores of the first few ordination axes or principal curve (Beck et al., 2018; Bennion et al., 2015).

822 Whilst this two-step approach is relatively easy to implement and builds on approaches that  
823 palaeoecologists already use to summarise multivariate stratigraphic data, it is best thought of  
824 as modelling changes in abundance or relative composition at the community level. It is less  
825 well suited to unpicking taxon-specific trends however, because the ordination step combines  
826 individual species information into latent variables (axes) that are linear combinations of *all*  
827 species and it is these latent variables that are then modelled using GAM.

## 828 5 Conclusions

829 Formal statistical estimation of trends in palaeoenvironmental data has been hampered by  
830 the nature of the data that comprise the time series; the uneven spacing of samples in time  
831 makes it, if not impossible, difficult to fit classical statistical time series models like ARIMA.  
832 This has led palaeoecologists and palaeolimnologists to either ignore statistical estimation of  
833 trends or fall back on basic statistical methods such as linear parametric and non-parametric  
834 correlations or simple linear regression models, where the assumptions of the method are  
835 often grossly violated by the dependencies inherent to time series data. GAMs, whilst similar  
836 to the popular LOESS smoother, provide a superior alternative approach to trend estimation in  
837 palaeoenvironmental time series. GAMs can estimate non-linear trends, provide estimates of  
838 the magnitude of change as well as allow the identification of periods of change, can account  
839 for the lack of independence (either via autocorrelation processes or via the fitting of a wiggly  
840 trend), and provide a formal framework for statistical inference on each of these features.

841 In presenting the GAM with specific palaeoenvironmental examples and addressing the issues  
842 that arise in palaeoenvironmental time series, it is hoped that palaeoecologists and palaeolim-  
843 nologists will be motivated to give greater consideration to the estimation of trends and the  
844 identification of change in stratigraphic time series.

## 845 Conflict of interest statement

846 The author declares that the research was conducted in the absence of any commercial or  
847 financial relationships that could be construed as a potential conflict of interest.

## 848 Acknowledgements

849 The ideas expressed in this paper are the result of many fruitful conversations with colleagues  
850 past and present at the Environmental Change Research Centre, UCL, and the University of  
851 Regina. In particular I am indebted to Helen Bennion, Rick Battarbee, and Peter Leavitt for  
852 their collaborations on projects over many years, and to David Miller, Eric Pedersen, and Noam  
853 Ross, my GAM workshop partners in crime. Without Simon Wood's *mgcv* software and his re-  
854 search on GAMs, the application of these models to palaeo time series would not be as straight  
855 forward. This work was supported by a Natural Sciences and Engineering Council of Canada  
856 (NSERC) Discovery Grant to the author (RGPIN-2014-04032).

## 857 References

- 858 Anchukaitis, K. J., and Tierney, J. E. (2013). Identifying coherent spatiotemporal modes in time-  
859 uncertain proxy paleoclimate records. *Climate Dynamics* 41, 1291–1306. doi:[10.1007/s00382-](https://doi.org/10.1007/s00382-012-1483-0)  
860 [012-1483-0](https://doi.org/10.1007/s00382-012-1483-0).
- 861 Beck, K. K., Fletcher, M.-S., Gadd, P. S., Heijnis, H., Saunders, K. M., Simpson, G. L., et al.  
862 (2018). Variance and Rate-of-Change as early warning signals for a critical transition in an  
863 aquatic ecosystem state: A test case from tasmania, australia. *Journal of Geophysical Research:*  
864 *Biogeosciences* 123, 2017JG004135. doi:[10.1002/2017JG004135](https://doi.org/10.1002/2017JG004135).
- 865 Bennion, H., Simpson, G. L., and Goldsmith, B. J. (2015). Assessing degradation and recovery  
866 pathways in lakes impacted by eutrophication using the sediment record. *Frontiers in Ecology*  
867 *and Evolution* 3. doi:[10.3389/fevo.2015.00094](https://doi.org/10.3389/fevo.2015.00094).
- 868 Bergmeir, C., Hyndman, R. J., and Koo, B. (2018). A note on the validity of cross-validation for  
869 evaluating autoregressive time series prediction. *Computational Statistics & Data Analysis* 120,  
870 70–83. doi:[10.1016/j.csda.2017.11.003](https://doi.org/10.1016/j.csda.2017.11.003).
- 871 Birks, H. J. B. (1998). Numerical tools in palaeolimnology — progress, potentialities, and prob-  
872 lems. *Journal of Paleolimnology* 20, 307–332. doi:[10.1023/A:1008038808690](https://doi.org/10.1023/A:1008038808690).
- 873 Birks, H. J. B. (2012a). “Introduction and overview of part III,” in *Tracking environmental change*  
874 *using lake sediments* (Springer, Dordrecht), 331–353. doi:[10.1007/978-94-007-2745-8\\_10](https://doi.org/10.1007/978-94-007-2745-8_10).
- 875 Birks, H. J. B. (2012b). “Overview of numerical methods in palaeolimnology,” in *Tracking envi-*  
876 *ronmental change using lake sediments* (Springer, Dordrecht), 19–92. doi:[10.1007/978-94-007-2745-](https://doi.org/10.1007/978-94-007-2745-8_2)  
877 [8\\_2](https://doi.org/10.1007/978-94-007-2745-8_2).
- 878 Blaauw, M., and Heegaard, E. (2012). “Estimation of Age-Depth relationships,” in *Tracking*  
879 *environmental change using lake sediments* (Springer, Dordrecht), 379–413. doi:[10.1007/978-94-](https://doi.org/10.1007/978-94-007-2745-8_12)  
880 [007-2745-8\\_12](https://doi.org/10.1007/978-94-007-2745-8_12).
- 881 Brassell, S. C. (1993). “Applications of biomarkers for delineating marine paleoclimatic fluctu-  
882 ations during the pleistocene,” in *Organic geochemistry: Principles and applications*, eds. M. H. En-  
883 gel and S. A. Macko (Boston, MA: Springer US), 699–738. doi:[10.1007/978-1-4615-2890-6\\_34](https://doi.org/10.1007/978-1-4615-2890-6_34).
- 884 Chu, G., Sun, Q., Li, S., Zheng, M., Jia, X., Lu, C., et al. (2005). Long-chain alkenone distribu-  
885 tions and temperature dependence in lacustrine surface sediments from china. *Geochimica et*  
886 *Cosmochimica Acta* 69, 4985–5003. doi:[10.1016/j.gca.2005.04.008](https://doi.org/10.1016/j.gca.2005.04.008).
- 887 Cleveland, W. S. (1979). Robust locally weighted regression and smoothing scatterplots. *Jour-*  
888 *nal of the American Statistical Association* 74, 829–836. doi:[10.1080/01621459.1979.10481038](https://doi.org/10.1080/01621459.1979.10481038).
- 889 Craven, P., and Wahba, G. (1978). Smoothing noisy data with spline functions. *Numerische*  
890 *Mathematik* 31, 377–403. doi:[10.1007/BF01404567](https://doi.org/10.1007/BF01404567).
- 891 Duchon, J. (1977). “Splines minimizing rotation-invariant semi-norms in sobolev spaces,”  
892 in *Constructive theory of functions of several variables* (Springer, Berlin, Heidelberg), 85–100.  
893 doi:[10.1007/BFb0086566](https://doi.org/10.1007/BFb0086566).
- 894 Dutilleul, P., Cumming, B. F., and Lontoc-Roy, M. (2012). “Autocorrelogram and periodogram  
895 analyses of palaeolimnological Temporal-Series from lakes in central and western north amer-

- 896 ica to assess shifts in drought conditions,” in *Tracking environmental change using lake sediments*  
897 (Springer, Dordrecht), 523–548. doi:[10.1007/978-94-007-2745-8\\_16](https://doi.org/10.1007/978-94-007-2745-8_16).
- 898 D’Andrea, W. J., Huang, Y., Fritz, S. C., and Anderson, N. J. (2011). Abrupt holocene climate  
899 change as an important factor for human migration in west greenland. *Proceedings of the National*  
900 *Academy of Sciences* 108, 9765–9769. doi:[10.1073/pnas.1101708108](https://doi.org/10.1073/pnas.1101708108).
- 901 Epperson, J. F. (1987). On the Runge example. *The American Mathematical Monthly* 94, 329–341.  
902 doi:[10.2307/2323093](https://doi.org/10.2307/2323093).
- 903 Fahrmeir, L., and Kneib, T. (2008). “On the identification of trend and correlation in temporal  
904 and spatial regression,” in *Recent advances in linear models and related areas* (Physica-Verlag HD),  
905 1–27. doi:[10.1007/978-3-7908-2064-5\\_1](https://doi.org/10.1007/978-3-7908-2064-5_1).
- 906 Fahrmeir, L., Kneib, T., Lang, S., and Marx, B. (2013). *Regression: Models, methods and applications*.  
907 Springer Berlin Heidelberg doi:[10.1007/978-3-642-34333-9](https://doi.org/10.1007/978-3-642-34333-9).
- 908 Gautheir, T. D. (2001). Detecting trends using spearman’s rank correlation coefficient. *Envi-*  
909 *ronmental Forensics* 2, 359–362. doi:[10.1080/713848278](https://doi.org/10.1080/713848278).
- 910 Glew, J. R., Smol, J. P., and Last, W. M. (2001). “Sediment core collection and extrusion,” in  
911 *Tracking environmental change using lake sediments: Basin analysis, coring, and chronological techniques*,  
912 eds. W. M. Last and J. P. Smol (Dordrecht: Springer Netherlands), 73–105. doi:[10.1007/0-306-](https://doi.org/10.1007/0-306-47669-X_5)  
913 [47669-X\\_5](https://doi.org/10.1007/0-306-47669-X_5).
- 914 Golding, N., and Purse, B. V. (2016). Fast and flexible bayesian species distribution modelling  
915 using gaussian processes. *Methods in Ecology and Evolution*. doi:[10.1111/2041-210X.12523](https://doi.org/10.1111/2041-210X.12523).
- 916 Handcock, M. S., Meier, K., and Nychka, D. (1994). Kriging and splines: An empirical compar-  
917 ison of their predictive performance in some applications: Comment. *Journal of the American*  
918 *Statistical Association* 89, 401–403. doi:[10.2307/2290838](https://doi.org/10.2307/2290838).
- 919 Hastie, T. J., and Tibshirani, R. J. (1990). *Generalized additive models*. Boca Raton, Fl.: Chapman  
920 & Hall / CRC.
- 921 Hastie, T., and Tibshirani, R. (1986). Generalized additive models. *Statistical Science* 1, 297–310.
- 922 Juggins, S., and Telford, R. J. (2012). “Exploratory data analysis and data display,” in *Tracking*  
923 *environmental change using lake sediments* (Springer, Dordrecht), 123–141. doi:[10.1007/978-94-](https://doi.org/10.1007/978-94-007-2745-8_5)  
924 [007-2745-8\\_5](https://doi.org/10.1007/978-94-007-2745-8_5).
- 925 Kammann, E. E., and Wand, M. P. (2003). Geoaddivitive models. *Journal of the Royal Statistical*  
926 *Society. Series C, Applied statistics* 52, 1–18. doi:[10.1111/1467-9876.00385](https://doi.org/10.1111/1467-9876.00385).
- 927 Kimeldorf, G. S., and Wahba, G. (1970). A correspondence between bayesian estimation on  
928 stochastic processes and smoothing by splines. *Annals of Mathematical Statistics* 41, 495–502.
- 929 Magee, L. (1998). Nonlocal behavior in polynomial regressions. *The American Statistician* 52,  
930 20–22. doi:[10.2307/2685560](https://doi.org/10.2307/2685560).
- 931 Mann, M. E. (2004). On smoothing potentially non-stationary climate time series. *Geophysical*  
932 *Research Letters* 31, L07214. doi:[10.1029/2004GL019569](https://doi.org/10.1029/2004GL019569).
- 933 Mann, M. E. (2008). Smoothing of climate time series revisited. *Geophysical Research Letters* 35,



- 934 L16708. doi:[10.1029/2008GL034716](https://doi.org/10.1029/2008GL034716).
- 935 Marra, G., and Wood, S. N. (2012). Coverage properties of confidence intervals for generalized  
936 additive model components. *Scandinavian Journal of Statistics, Theory and Applications* 39, 53–74.  
937 doi:[10.1111/j.1467-9469.2011.00760.x](https://doi.org/10.1111/j.1467-9469.2011.00760.x).
- 938 McCullagh, P., and Nelder, J. A. (1989). *Generalized linear models, second edition*. CRC Press.
- 939 Mills, T. C. (2006). Modelling current trends in Northern Hemisphere temperatures. *International  
940 Journal of Climatology* 26, 867–884. doi:[10.1002/joc.1286](https://doi.org/10.1002/joc.1286).
- 941 Mills, T. C. (2007). A note on trend decomposition: The “classical” approach revisited  
942 with an application to surface temperature trends. *Journal of Applied Statistics* 34, 963–972.  
943 doi:[10.1080/02664760701590418](https://doi.org/10.1080/02664760701590418).
- 944 Mills, T. C. (2010). “Skinning a cat”: Alternative models of representing temperature trends.  
945 *Climatic Change* 101, 415–426.
- 946 Nychka, D. (1988). Bayesian confidence intervals for smoothing splines. *Journal of the American  
947 Statistical Association* 83, 1134–1143. doi:[10.1080/01621459.1988.10478711](https://doi.org/10.1080/01621459.1988.10478711).
- 948 PAGES 2K Consortium (2013). Continental-scale temperature variability during the past two  
949 millennia. *Nature Geoscience* 6, 339–346. doi:[10.1038/ngeo1797](https://doi.org/10.1038/ngeo1797).
- 950 Pinheiro, J. C., and Bates, D. M. (2000). *Mixed-Effects models in S and S-PLUS*. Springer Science  
951 & Business Media.
- 952 Pya, N. (2017). *Scam: Shape constrained additive models*. Available at: [https://CRAN.R-project.  
953 org/package=scam](https://CRAN.R-project.org/package=scam).
- 954 Pya, N., and Wood, S. N. (2015). Shape constrained additive models. *Statistics and Computing*  
955 25, 543–559. doi:[10.1007/s11222-013-9448-7](https://doi.org/10.1007/s11222-013-9448-7).
- 956 Pya, N., and Wood, S. N. (2016). A note on basis dimension selection in generalized additive  
957 modelling. *ArXiv e-prints*.
- 958 R Core Team (2017). *R: A language and environment for statistical computing*. Vienna, Austria: R  
959 Foundation for Statistical Computing Available at: <https://www.R-project.org/>.
- 960 R Core Team (2018). *R: A language and environment for statistical computing*. Vienna, Austria: R  
961 Foundation for Statistical Computing Available at: <https://www.R-project.org/>.
- 962 Rasmussen, C. E., and Williams, C. K. I. (2006). *Gaussian processes for machine learning*. MIT  
963 Press.
- 964 Reiss, P. T., and Ogden, R. T. (2009). Smoothing parameter selection for a class of semipara-  
965 metric linear models. *Journal of the Royal Statistical Society. Series B, Statistical methodology* 71,  
966 505–523. doi:[10.1111/j.1467-9868.2008.00695.x](https://doi.org/10.1111/j.1467-9868.2008.00695.x).
- 967 Runge, C. (1901). Über empirische funktionen und die interpolation zwischen äquidistanten  
968 ordinaten. *Zeitschrift für Angewandte Mathematik und Physik* 46, 224–243.
- 969 Ruppert, D., Wand, M. P., and Carroll, R. J. (2003). *Semiparametric Regression*. Cambridge Uni-  
970 versity Press.
- 971 Silverman, B. W. (1985). Some aspects of the spline smoothing approach to non-parametric

- 972 regression curve fitting. *Journal of the Royal Statistical Society. Series B, Statistical methodology* 47,  
973 1–52.
- 974 Smol, J. P. (2008). *Pollution of lakes and rivers: A paleoenvironmental perspective*. Blackwell Pub.
- 975 Smol, J. P., Birks, H. J. B., Lotter, A. F., and Juggins, S. (2012). “The march towards the quanti-  
976 tative analysis of palaeolimnological data,” in *Tracking environmental change using lake sediments*  
977 (Springer, Dordrecht), 3–17. doi:[10.1007/978-94-007-2745-8\\_1](https://doi.org/10.1007/978-94-007-2745-8_1).
- 978 Tian, J., Nelson, D. M., and Hu, F. S. (2011). How well do sediment indicators record past  
979 climate? An evaluation using annually laminated sediments. *Journal of Paleolimnology* 45, 73–  
980 84. doi:[10.1007/s10933-010-9481-x](https://doi.org/10.1007/s10933-010-9481-x).
- 981 Toney, J. L., Huang, Y., Fritz, S. C., Baker, P. A., Grimm, E., and Nyren, P. (2010). Cli-  
982 matic and environmental controls on the occurrence and distributions of long chain  
983 alkenones in lakes of the interior united states. *Geochimica et Cosmochimica Acta* 74, 1563–1578.  
984 doi:[10.1016/j.gca.2009.11.021](https://doi.org/10.1016/j.gca.2009.11.021).
- 985 Wahba, G. (1983). Bayesian “confidence intervals” for the Cross-Validated smoothing spline.  
986 *Journal of the Royal Statistical Society. Series B, Statistical methodology* 45, 133–150.
- 987 Wahba, G. (1990). *Spline models for observational data*. SIAM.
- 988 Wang, Y., Naumann, U., Wright, S. T., and Warton, D. I. (2012). Mvabund– an R package for  
989 model-based analysis of multivariate abundance data. *Methods in Ecology and Evolution* 3, 471–  
990 474. doi:[10.1111/j.2041-210X.2012.00190.x](https://doi.org/10.1111/j.2041-210X.2012.00190.x).
- 991 Warton, D. I. (2011). Regularized sandwich estimators for analysis of high-dimensional  
992 data using generalized estimating equations. *Biometrics* 67, 116–123. doi:[10.1111/j.1541-  
993 0420.2010.01438.x](https://doi.org/10.1111/j.1541-0420.2010.01438.x).
- 994 Warton, D. I., Blanchet, F. G., O’Hara, R. B., Ovaskainen, O., Taskinen, S., Walker, S. C., et al.  
995 (2015). So many variables: Joint modeling in community ecology. *Trends in Ecology & Evolution*.  
996 doi:[10.1016/j.tree.2015.09.007](https://doi.org/10.1016/j.tree.2015.09.007).
- 997 Warton, D. I., Wright, S. T., and Wang, Y. (2012). Distance-based multivariate analy-  
998 ses confound location and dispersion effects. *Methods in Ecology and Evolution* 3, 89–101.  
999 doi:[10.1111/j.2041-210X.2011.00127.x](https://doi.org/10.1111/j.2041-210X.2011.00127.x).
- 1000 Wood, S. N. (2003). Thin plate regression splines. *Journal of the Royal Statistical Society. Series B,*  
1001 *Statistical methodology* 65, 95–114. doi:[10.1111/1467-9868.00374](https://doi.org/10.1111/1467-9868.00374).
- 1002 Wood, S. N. (2004). Stable and efficient multiple smoothing parameter estimation for  
1003 generalized additive models. *Journal of the American Statistical Association* 99, 673–686.  
1004 doi:[10.2307/27590439](https://doi.org/10.2307/27590439).
- 1005 Wood, S. N. (2011). Fast stable restricted maximum likelihood and marginal likelihood estima-  
1006 tion of semiparametric generalized linear models. *Journal of the Royal Statistical Society. Series B,*  
1007 *Statistical methodology* 73, 3–36. doi:[10.1111/j.1467-9868.2010.00749.x](https://doi.org/10.1111/j.1467-9868.2010.00749.x).
- 1008 Wood, S. N. (2017). *Generalized Additive Models: An Introduction with R, Second edition*. CRC Press.
- 1009 Wood, S. N., Pya, N., and Säfken, B. (2016). Smoothing parameter and model selection  
1010 for general smooth models. *Journal of the American Statistical Association* 111, 1548–1563.

1011 doi:[10.1080/01621459.2016.1180986](https://doi.org/10.1080/01621459.2016.1180986).

1012 Yee, T. W., and Mitchell, N. D. (1991). Generalized additive models in plant ecology. *Journal of*  
1013 *Vegetation Science* 2, 587–602. doi:[10.2307/3236170](https://doi.org/10.2307/3236170).

1014 Zink, K.-G., Leythaeuser, D., Melkonian, M., and Schwark, L. (2001). Temperature de-  
1015 pendency of long-chain alkenone distributions in recent to fossil limnic sediments and  
1016 in lake waters11Associate editor: J. b. fein. *Geochimica et Cosmochimica Acta* 65, 253–265.  
1017 doi:[10.1016/S0016-7037\(00\)00509-3](https://doi.org/10.1016/S0016-7037(00)00509-3).

## 1018 Appendix 1 — Simultaneous intervals

1019 We proceed by considering a simultaneous confidence interval for a function  $f(x)$  at a set of  $M$   
1020 locations in  $x$ ; we'll refer to these locations, following the notation of Ruppert et al. (2003) by

$$\mathbf{g} = (g_1, g_2, \dots, g_M)$$

1021 The true function over  $\mathbf{g}$ ,  $\mathbf{f}_{\mathbf{g}}$ , is defined as the vector of evaluations of  $f$  at each of the  $M$  locations

$$\mathbf{f}_{\mathbf{g}} \equiv \begin{bmatrix} f(g_1) \\ f(g_2) \\ \vdots \\ f(g_M) \end{bmatrix}$$

1022 and the corresponding estimate of the true function given by the fitted GAM denoted by  $\hat{\mathbf{f}}_{\mathbf{g}}$ .  
1023 The difference between the true function and our unbiased estimator is given by

$$\hat{\mathbf{f}}_{\mathbf{g}} - \mathbf{f}_{\mathbf{g}} = \mathbf{C}_{\mathbf{g}} \begin{bmatrix} \hat{\boldsymbol{\beta}} - \boldsymbol{\beta} \\ \hat{\mathbf{u}} - \mathbf{u} \end{bmatrix},$$

1024 where  $\mathbf{C}_{\mathbf{g}}$  is a matrix formed by the evaluation of the basis functions at locations  $\mathbf{g}$ , and the part  
1025 in square brackets is the bias in the estimated model coefficients, which we assume to be mean 0  
1026 and distributed, approximately, multivariate normal with mean vector  $\mathbf{0}$  and covariance matrix  
1027  $\mathbf{V}_{\mathbf{b}}$

$$\begin{bmatrix} \hat{\boldsymbol{\beta}} - \boldsymbol{\beta} \\ \hat{\mathbf{u}} - \mathbf{u} \end{bmatrix} \text{approx. } \underset{\sim}{N}(\mathbf{0}, \mathbf{V}_{\mathbf{b}}),$$

1028 where  $\mathbf{V}_{\mathbf{b}}$  is the Bayesian covariance matrix of the GAM coefficients.

1029 Now, the  $(1 - \alpha)100\%$  simultaneous confidence interval is

$$\hat{\mathbf{f}}_{\mathbf{g}} \pm m_{1-\alpha} \begin{bmatrix} \widehat{\text{st.dev}}(\hat{f}(g_1) - f(g_1)) \\ \widehat{\text{st.dev}}(\hat{f}(g_2) - f(g_2)) \\ \vdots \\ \widehat{\text{st.dev}}(\hat{f}(g_M) - f(g_M)) \end{bmatrix},$$

1030 where  $m_{1-\alpha}$  is the  $1 - \alpha$  quantile of the random variable

$$\sup_{x \in \mathcal{X}} \left| \frac{\hat{f}(x) - f(x)}{\widehat{\text{st.dev}}(\hat{f}(x) - f(x))} \right| \approx \max_{1 \leq \ell \leq M} \left| \frac{\left( \mathbf{C}_{\mathbf{g}} \begin{bmatrix} \hat{\beta} - \beta \\ \hat{\mathbf{u}} - \mathbf{u} \end{bmatrix} \right)_{\ell}}{\widehat{\text{st.dev}}(\hat{f}(g_{\ell}) - f(g_{\ell}))} \right|$$

1031 The sup refers to the *supremum* or the *least upper bound*; this is the least value of  $\mathcal{X}$ , the set of all  
1032 values of which we observed subset  $x$ , that is *greater* than all of the values in the subset. Often  
1033 this is the maximum value of the subset. This is what is indicated by the right-hand side of  
1034 the equation; we want the maximum (absolute) value of the ratio over all values in  $\mathbf{g}$ .

1035 The fractions in both sides of the equation correspond to the standardized deviation between  
1036 the true function and the model estimate, and we consider the *maximum absolute* standardized  
1037 deviation. We don't usually know the distribution of the maximum absolute standardized  
1038 deviation but we need this to access its quantiles. However, we can closely approximate the  
1039 distribution via simulation. The difference here is that rather than simulating from the poste-  
1040 rior of the model as we did earlier [see section Confidence intervals](#), this time we simulate from  
1041 the multivariate normal distribution with mean vector  $\mathbf{0}$  and covariance matrix  $\mathbf{V}_{\mathbf{b}}$ . For each  
1042 simulation we find the maximum absolute standardized deviation of the fitted function from  
1043 the true function over the grid of  $x$  values we are considering. Then we collect all these max-  
1044 ima, sort them and either take the  $1 - \alpha$  probability quantile of the maxima, or the maximum  
1045 with rank  $\lceil (1 - \alpha)/N \rceil$ .